

8/78 HP  
CM

c29

# Quiet Clean Short-Haul Experimental Engine (QCSEE)

## Over-The-Wing (OTW) Propulsion System Test Report

### Volume II - Aerodynamics and Performance

(NASA-CR-135324) QUIET CLEAN SHORT-HAUL N80-14120  
EXPERIMENTAL ENGINE (QCSEE) OVER-THE-WING  
(OTW) PROPULSION SYSTEM TEST REPORT. VOLUME  
2: AERODYNAMICS AND PERFORMANCE (General Unclas  
Electric Co.) 49 p HC A03/MF A01 CSCL 21E G3/07 33510

by

Advanced Engineering and Technology Programs Department

GENERAL ELECTRIC COMPANY

July 1978

Prepared For

National Aeronautics and Space Administration



NASA-Lewis Research Center

NAS3-18021

SQT

Prelaunch  
Mission Operation Report  
O-491-203-81-03

TO: A/Administrator 1981

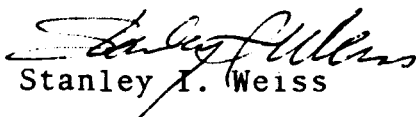
FROM: O/Associate Administrator for Space Transportation  
Operations

SUBJECT: INTELSAT V-C (F-3) Launch

The third in a series of improved INTELSAT commercial communications satellites will be launched by an Atlas-Centaur (AC-55) from the Eastern Space and Missile Center (ESMC) no earlier than December 9, 1981. The INTELSAT V series has a capacity of 12,000 voice circuits plus two television channels.

The INTELSAT Global Satellite System comprises two elements: the space segment, consisting of satellites owned by INTELSAT positioned over the Atlantic, Indian, and Pacific Ocean regions; and the ground segment, consisting of Earth stations owned by telecommunications entities in the countries in which they are located.

INTELSAT awarded a contract for the development and manufacture of INTELSAT V satellites to Ford Aerospace and Communications Corporation as a prime contractor, and an international team of manufacturers as subcontractors. A number of follow-on satellites with modified and expanded communications capabilities are being considered.

  
Stanley I. Weiss



NOTICE: This document may be exempt from public disclosure under the Freedom of Information Act (5 U.S.C. 552). Requests for its release to persons outside the U.S. Government should be handled under the provisions of NASA Policy Directive 1382.2.

N82-13162

Unclas  
G3/15 08440

CSSL 22B

(NASA-TM-84072) MISSION OPERATION REPORT:  
INTELSAT V-C (F-3) (National Aeronautics and  
Space Administration) 22 p HC A02/MF A01



National Aeronautics and  
Space Administration

ORIGINAL PAGE IS  
OF PCCR QUALITY

# Mission Operation Report

OFFICE OF SPACE TRANSPORTATION OPERATIONS Report No. O-491-203-81 03



INTELSAT V-C(F-3)

## **FOREWORD**

MISSION OPERATION REPORTS are published expressly for the use of NASA Senior Management, as required by the Administrator in NASA Management Instruction HQMI 8610.1A, effective October 1, 1974. The purpose of these reports is to provide NASA Senior Management with timely, complete, and definitive information on flight mission plans, and to establish official Mission Objectives which provide the basis for assessment of mission accomplishment.

Prelaunch reports are prepared and issued for each flight project just prior to launch. Following launch, updating (Post Launch) reports for each mission are issued to keep General Management currently informed of definitive mission results as provided in NASA Management Instruction HQMI 8610.1A.

Primary distribution of these reports is intended for personnel having program/project management responsibilities which sometimes result in a highly technical orientation. The Office of Public Affairs publishes a comprehensive series of reports on NASA flight mission which are available for dissemination to the Press.

Published and Distributed by  
HEADQUARTERS ADMINISTRATION DIVISION  
NASA HEADQUARTERS

CONTENTS

	<u>Page</u>
General.....	1
Mission Objectives for INTELSAT V-C (F-3).....	4
Spacecraft Description.....	5
Launch Vehicle Description.....	14
INTELSAT Team.....	16

LIST OF FIGURES

<u>Figure No.</u>	<u>Title</u>	<u>Page</u>
1	INTELSAT V Spacecraft	6
2	Mission Summary	8
3	INTELSAT V Launch Vehicle	

LIST OF TABLES

<u>Table No.</u>		<u>Page</u>
1	INTELSAT Member Countries	2
2	Launch Vehicle Characteristics	15

## GENERAL

The International Telecommunications Satellite Organization (INTELSAT) headquartered in Washington, DC, was created on August 20, 1964, through the adoption of interim agreements signed by 11 countries, for the establishment of a global commercial communications satellite system.

Since February 12, 1973, INTELSAT has operated under definitive agreements with an organizational structure consisting of: (a) an Assembly of Parties (governments that are Parties to the INTELSAT Agreement); (b) a Meeting of Signatories (governments or their designated telecommunications entities that have signed the Operating Agreement); (c) a Board of Governors; and (d) an Executive Organ headed by a Director General, Mr. Santiago Astrain.

The Board of Governors, which has overall responsibility for the decisions relating to the design, development, construction, establishment, operating, and maintenance of the INTELSAT space segment, is currently composed of 27 Governors representing 83 Signatories.

The INTELSAT global satellite system comprises two essential elements: the space segment, consisting of satellites owned by INTELSAT, and the ground segment, consisting of Earth stations, owned by telecommunications entities in the countries in which they are located.

At present, the space segment consists of 10 satellites in synchronous orbit at an altitude of approximately 35,780 km (22,240 miles). Global service is provided through a combination of INTELSAT IV-A and INTELSAT IV satellites over the Atlantic, Indian, and Pacific Ocean regions.

The INTELSAT IV-A has a capacity of 6,000 voice circuits and two television channels, while the INTELSAT IV has a capacity of 4,000 voice circuits plus two television channels. The INTELSAT V has a capacity of 12,000 voice circuits plus two television channels.

The ground segment of the global system consists of 295 communications antennas at 242 Earth station sites in 129 countries and territories.

The combined system of satellites and Earth stations provides more than 800 Earth station-to-Earth station communications pathways.

In addition to the international voice circuits in full-time use (now about 8,500), INTELSAT provides a wide variety of telecommunications services, including telegraph, telex, data, and television to over 150 countries, territories, and possessions (Table 1).

TABLE 1

INTELSAT MEMBER COUNTRIES

Afghanistan	Haiti	Pakistan
Algeria	Honduras	Panama
Angola	Iceland	Paraguay
Argentina	India	Peru
Australia	Indonesia	Philippines
Austria	Iran, Islamic Republic of	Portugal
Bangladesh	Iraq	Qatar
Barbados	Ireland	Saudi Arabia
Belgium	Israel	Senegal
Bolivia	Italy	Singapore
Brazil	Ivory Coast	South Africa
Cameroon	Jamaica	Spain
Canada	Japan	Sri Lanka
Central African Republic	Jordan	Sudan
Chad	Kenya	Sweden
Chile	Korea, Republic of	Switzerland
China, People's Republic of	Kuwait	Syria
Colombia	Lebanon	Tanzania
Congo	Libya	Thailand
Costa Rica	Liechtenstein	Trinidad and Tobago
Cyprus	Luxembourg	Tunisia
Denmark	Madagascar	Turkey
Dominican Republic	Malaysia	Uganda
Ecuador	Mali	United Arab Emirates
Egypt	Mauritania	United Kingdom
El Salvador	Mexico	United States
Ethiopia	Monaco	Upper Volta
Fiji	Morocco	Vatican City State
Finland	Netherlands	Venezuela
France	New Zealand	Viet Nam
Gabon	Nicaragua	Yemen Arab Republic
Germany, Federal Republic of	Niger	Yugoslavia
Ghana	Nigeria	Zaire
Greece	Norway	Zambia
Guatemala	Oman	
Guinea, People's Revolutionary Republic of		

INTELSAT NON-SIGNATORY USERS

Bahrain	Kiribati	Romania
Botswana	Liberia	Seychelles
Brunei	Malawi	Sierra Leone
Burma	Maldives	Solomon Islands
Cook Islands	Mauritius	Somalia
Czechoslovakia	Mozambique	Surinam
Cuba	Nauru, Republic of	Togo
Djibouti	New Guinea	Tonga
Gambia	Papua	U.S.S.R.
Guyana	Poland	Western Samoa
Hungary		

OTHER TERRITORY USERS

American Samoa	French Guiana	Netherlands Antilles
Ascension Island	French Polynesia	New Caledonia
Azores	French West Indies	Van Uatu
Belize	Gibraltar	
Bermuda	Guam	
Cayman Islands	Hong Kong	



Fifteen countries also lease satellite capacity from INTELSAT for their own domestic communications. These are: Algeria, Australia, Brazil, Chile, Colombia, France, India, Nigeria, Norway, Oman, Peru, Saudi Arabia, Spain, Sudan, and Zaire.

INTELSAT currently authorizes two standards for Earth stations that operate international services through its satellites: Standard A, with 30-meter (100 ft.) or larger, dish antenna, 10 stories tall, which can be rotated one degree per second and which can track to within a fraction of a degree a satellite stationed in synchronous orbit; and a smaller Standard B of 10 meters (33 ft.).


MISSION OBJECTIVES FOR INTELSAT V-C (F-3)

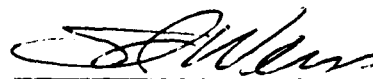
NASA OBJECTIVE

To launch the INTELSAT V-C (F-3) satellite into a transfer orbit which enables the spacecraft apogee motor to inject the spacecraft into a synchronous orbit.

COMSAT OBJECTIVES

To fire the apogee motor, position the satellite into its planned geostationary position, and operate and manage the system for INTELSAT.

  
 Joseph B. Mahon  
 Director, Expendable Launch  
 Vehicle Programs

  
 Stanley I. Weiss  
 Associate Administrator for  
 Space Transportation Operations

Date: December 1, 1981

Date: Dec 1, 1981

## SPACECRAFT DESCRIPTION

Figures collected as a result of INTELSAT-sponsored Global Telecommunications Traffic Conference indicated that an INTELSAT IV-A satellite would have insufficient capacity to cope with the traffic and load on the Atlantic Ocean primary satellite and on the Indian Ocean satellite by the early 1980s.

While one solution could have been simply to orbit another INTELSAT IV-A Atlantic Ocean and Indian Ocean satellite, subsequent planning proceeded towards the development of a high-capacity INTELSAT V satellite (Figure 1). After an international bidding process, the INTELSAT Board of Governors, at its meeting in September 1976, decided to award a contract for the development and manufacture of seven INTELSAT V satellites to Ford Aerospace and Communications Corporation as prime contractor, and an international team of manufacturers as subcontractors. Since that time, the Board has decided to order two additional INTELSAT V satellites and is considering an order for a number of follow-on spacecraft with modified and expanded communications capabilities.

### AN INTERNATIONAL EFFORT

Contributions have been made to the design, development, and manufacture of INTELSAT V by aerospace manufacturers around the world, under the prime contractor Ford Aerospace and Communications Corporation (FACC) of the United States.

Members of this international manufacturing team include:

- . Aerospatiale (France)
- . GEC-Marconi (United Kingdom)
- . Messerschmitt-Bolkow-Blohm (Federal Republic of Germany)
- . Mitsubishi Electric Corporation (Japan)
- . Selenia (Italy)
- . Thomson-CSF (France)

Each manufacturer has concentrated on specific areas of the INTELSAT program.

- . Aerospatiale (France) - Aerospatiale initiated the structural design that forms the main member of the spacecraft modular design construction. It supplies the main body structure thermal analysis and control.
- . GEC-Marconi (United Kingdom) - Marconi produces the 11 GHz beacon transmitter used for Earth station antenna tracking.

INTELSAT V SPACECRAFT

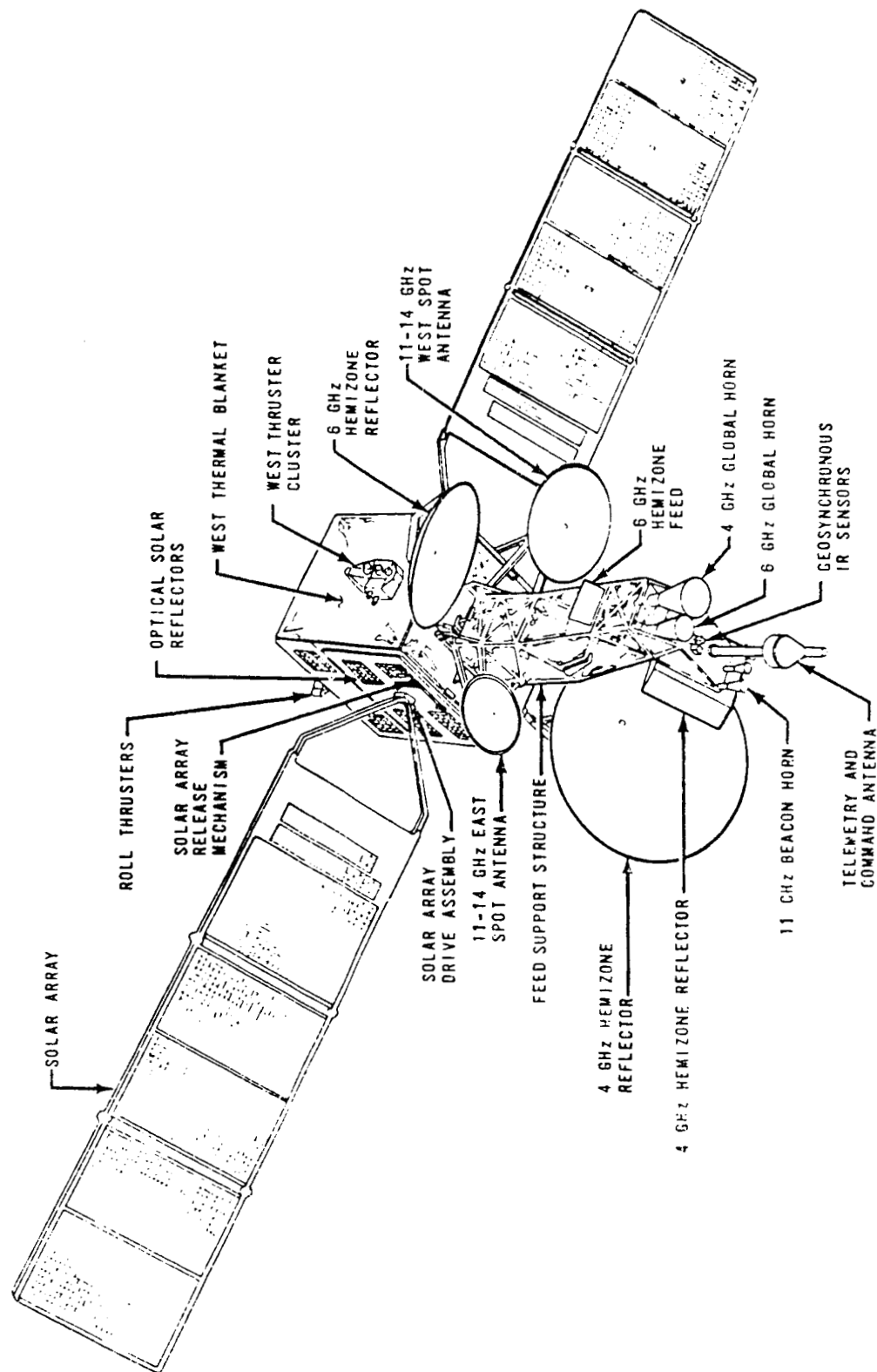


Fig. 1

- . Messerschmitt-Bolkow-Blohm (Federal Republic of Germany) - MBB designed and produces the satellite's control subsystem and the solar array.
- . Mitsubishi Electric Corporation (Japan) - Mitsubishi is responsible for both the 6 GHz and the 4 GHz Earth coverage antennas. It also manufactures the power control electronics and, from an FACC design, the telemetry and command digital units.
- . Selenia (Italy) - Selenia designed and built the six telemetry, command, and ranging antennas, two 11 GHz beacon antennas and two 14/11 GHz spot beam antennas. It also built the command receiver and telemetry transmitter which combine to form a ranging transponder for determination of the spacecraft position in transfer orbit.
- . Thomson-CSF (France) - Thomson built the 10 w, 11 GHz traveling wave tubes of which there are 10 per spacecraft.

All this is brought together by FACC through its Western Development Labs Division in Palo Alto, California. Ford is also responsible for the development of the satellite's communications package and for the development of the maritime communications subsystem (MCS) to be integrated into the fifth, sixth, seventh, eighth, and ninth INTELSAT V satellites. An INTELSAT V Mission Summary is shown on Figure 2.

## FACTS, STATISTICS, AND SPECIAL FEATURES

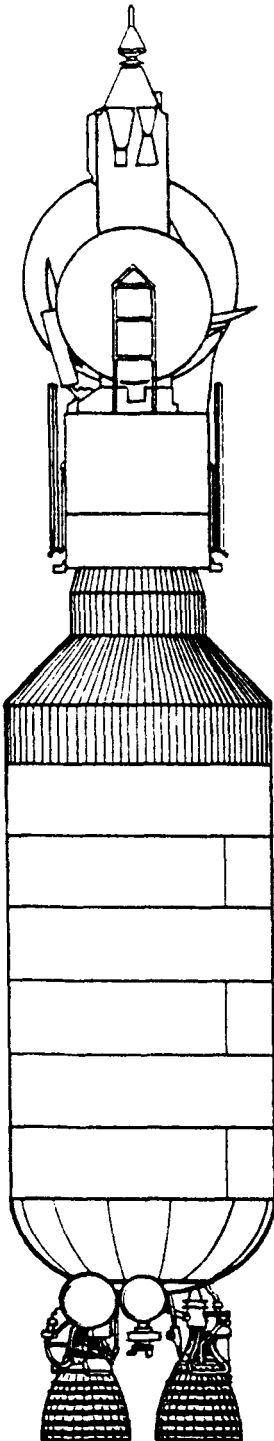
### Dimensions

- |                                   |   |
|-----------------------------------|---|
| . Solar Array (end to end)        | : 15.6 meters (51.1 feet)                             |
| . Main Body "Box"                 | : 1.66 x 2.01 x 1.77 meters<br>(5.4 x 6.6 x 5.8 feet) |
| . Height                          | : 6.4 meters (21.0 feet)                              |
| . Width (fully deployed)          | : 6.8 meters (22.25 feet)                             |
| . Weight (at launch, without MCS) | : 1,928 kilos (4,251 pounds)                          |

### General Characteristics

- . Three-axis body stabilized with Sun and Earth sensors and momentum wheel.
- . Wing-like, Sun-oriented solar array panels producing a total of 1,241 watts of electrical power after 7 years in orbit.
- . Modular construction.
- . Seven-year expected life in orbit.

## MISSION SUMMARY



## MISSION PARAMETERS

Mission Designation  
Mission Objective  
  
Mission Final Orbit  
Final Stationary Position

INTELSAT V Series  
Placement of commercial communications satellites into Earth stationary orbit. Stationary in Earth equatorial plane. To be selected by INTELSAT (desired positioning achieved by combined use of multiple revolutions in launch transfer orbit plus post-apogee drift orbit).

## LAUNCH PHASE PARAMETERS

Launch Mode  
Launch Azimuth  
Ascent Yaw Maneuver

Parking Orbit Ascent (Two Burn)  
97.6 degrees  
Small left yaw (to reduce P.O. inclination)

## CENTAUR PARKING ORBIT

Perigee/Apogee Altitude  
Orbit Inclination  
Coast Time in Orbit

80/193 nautical miles  
28.3 degrees  
14.2 minutes

## CENTAUR SECOND BURN

Location of Burn  
Burnout Altitude (MECO2)

First equatorial crossing  
95.2 nautical miles

## SPACECRAFT TRANSFER ORBIT

Perigee/Apogee Altitude  
Orbit Inclination  
Coast Time to 1st Apogee  
Orbit Period

90/19,324 nautical miles  
24.1 degrees (for 4206 lb S/C)  
5.20 hours (from S/C separation)  
633.8 minutes (at 1st apogee)

## SPACECRAFT APOGEE BURN

Location of Burn and  
Burnout Longitude

INTELSAT will command S/C apogee burn via RF link at one of the transfer orbit apogee occurrences (yet to be selected).

## SPACECRAFT FINAL ORBIT

Perigee/Apogee Altitude  
Orbit Inclination  
Orbit Period

19,324/19,324 nautical miles\*  
0 degrees\*  
23.935 hours

\* Nominal parameters for Earth stationary orbit. Actual INTELSAT V spacecraft final orbits may have slight variations in altitude and/or inclination angles.

Fig. 2

Communications Characteristics

- . Capacity average 12,000 simultaneous two-way telephone circuits and two television channels.
- . Utilizes both 14/11 GHz frequency band and 6/4 GHz frequency band.
- . The 14/11 GHz frequency band is used twice through east and west spot beams.
- . Six communications antennas - two global coverage horns, two hemispherical/zone offset-fed reflectors and two offset-fed spot beam reflectors.

SPACECRAFT

- . Aluminum main body structure.
- . Graphite epoxy antenna tower.
- . Catalytical and electro-thermal hydrazine thrusters.

INTELSAT FIRSTS

INTELSAT V is the first INTELSAT satellite to have the following features:

- . Frequency reuse through both spatial isolation and dual polarization isolation.
- . Multi-band communications - both 14/11 GHz and 6/4 GHz.
- . A contiguous band output multiplexer.
- . Maritime communications subsystem (MCS).
- . Use of nickel hydrogen batteries in later spacecraft.

COMMUNICATIONS CAPACITY

In designing INTELSAT V, engineers had to work within a number of limiting factors to achieve the communications capacity required.

Typical of these were:

- . limitations on the available frequency bands;
- . the maximum mass which could be placed in orbit by the then (1973+) only available launch vehicle - Atlas Centaur.

These limitations have been overcome with the result that each INTELSAT V will have twice the capacity of its predecessors. The extra capacity was derived by reusing the available frequency bandwidth - up to four times - and by utilizing another range of frequencies.

INTELSAT IV-A makes limited use of zonal beam antennas to increase its capacity by reusing frequencies twice. Of the 500 MHz bandwidth available to INTELSAT IV-A, a portion is allocated to global coverage transmissions and the remaining bandwidth is used twice in two hemispherical beams which are concentrated over heavy traffic areas. As these beams do not overlap, except with the global coverage beam, there is no possibility of signals in one beam interfering with signals in the other, even though they are on the same frequencies.

With INTELSAT V, frequency reuse techniques have been taken even further with the introduction of polarized transmissions. Overlaid on INTELSAT V's global beam transmissions are two circularly polarized transmissions beamed into separate hemispheres. Overlaid upon each of these, using the same frequencies but polarized in the opposite directions (orthogonal to the hemisphere transmissions), are two zonal beam transmissions. All of these beams operate using and reusing the frequencies in the 6/4 GHz band. In addition, there are concentrated spot beam transmissions using, for the first time for INTELSAT, frequencies in the 14/11 GHz (Ku) band.

#### MARITIME COMMUNICATIONS SUBSYSTEM (MCS)

For the first time, INTELSAT will build facilities for maritime communications services into several of its INTELSAT V satellites. The INTELSAT Board of Governors, at its meeting in January 1979, decided to go ahead with plans to install equipment designed to provide maritime communications services on board the fifth, sixth, seventh, eighth, and ninth in its series of INTELSAT V international communications satellites. The satellites carrying the MCS are to be placed in orbit commencing during 1982. It is planned that the maritime-equipped INTELSAT Vs will become part of a global system operated by the newly formed International Maritime Satellite Organization (INMARSAT). In this system, the INTELSAT Vs, as well as performing their normal international communications roles, would provide ship/shore/ship communications and other services. The maritime packages for the INTELSAT Vs are being developed and built by the Ford Aerospace and Communications Corporation, prime contractor for the INTELSAT V series satellites. INTELSAT has offered to lease the maritime communications facilities to INMARSAT over a 7 year lifetime. The INMARSAT system is expected to become the successor to the MARISAT system, currently being operated by the U.S. corporation, COMSAT General.



SPACECRAFT SUBSYSTEMSCommunications Repeater

The communications subsystem receives and amplifies signals from Earth, routes the signals between antenna beams, and retransmits the signals back to Earth. The equipment involved includes 15 receivers, 43 traveling wave tube amplifiers, and more than 140 microwave switches. The repeater provides 27 separate transponders which may be connected in nearly 600 different combinations of coverage areas and frequency bands. Solid state receivers, graphite epoxy filters, and contiguous channel output multiplexers are among the technical innovations introduced in this subsystem.

Communication Antennas

The antennas employ such advanced design features as dual-polarized low-axial ratio feed elements and extremely lightweight feed distribution networks. These items, as well as the antenna tower and reflectors, are made of graphite epoxy for extremely low weight and high temperature stability.

**COMMUNICATIONS PAYLOAD**

Quantity	Component	Remarks
<u>Communications Antennas</u>		
2	Offset fed, shaped beam frequency reuse antennas	Freq: 6/4 GHz Size: 2.44 and 1/6 m dia.
2	Offset fed, mechanically steered spot antennas	Freq: 14/11 GHz Size: 0.96 and 1.12 m dia.
2	Earth coverage horns	Freq: 6/4 GHz
1	Beacon antenna	Freq: 11 GHz
<u>Receivers</u>		All solid-state
4	14 GHz	2 active, 2 redundant
11	6 GHz	5 active, 6 redundant
<u>Traveling Wave Tubes</u>		
10	11 GHz, 10 w dual collectors	6 active, 4 redundant
33	4 GHz, 4.5 w and 8.5w	21 active, 12 redundant
<u>Upconverters</u>		
10	4/11 GHz	6 active, 4 redundant
<u>Transmitters</u>		
2	Beacon	Freq: 11.196 and 11.454 GHz

### Telemetry, Tracking and Command

The telemetry, tracking, and command subsystem is used to control the spacecraft during transfer orbit and on-station operations. The major elements of the subsystem include antennas, telemetry and command units, and a transponder.

Antennas are packaged in a single assembly except for the two telemetry Earth coverage horns. Two command antennas receive signals from Earth and three transmit antennas telemeter spacecraft data back to Earth.

The command subsystem provides for remote control from Earth of many spacecraft functions through a microwave link consisting of two ring slot antennas, two command receivers, and two command units. Diagnostic data and subsystem status are transmitted to the ground via two independent and redundant telemetry channels.

### Attitude Control

The attitude control subsystem provides active stabilization of the spacecraft. In transfer orbit, the spacecraft is spin-stabilized. Its attitude is derived from Earth sensor and Sun sensor data, processed by the attitude determination and control electronics.

After injection into synchronous orbit, the spacecraft is despun and the solar arrays and antenna reflectors deployed. In a series of maneuvers, it is then locked onto the correct attitude in relation to the Earth. In the normal on-station mode, pitch control is maintained by a spinning momentum wheel. Roll and yaw control is accomplished by firing small hydrazine thrusters. Three geostationary infrared sensors provide Earth reference data.

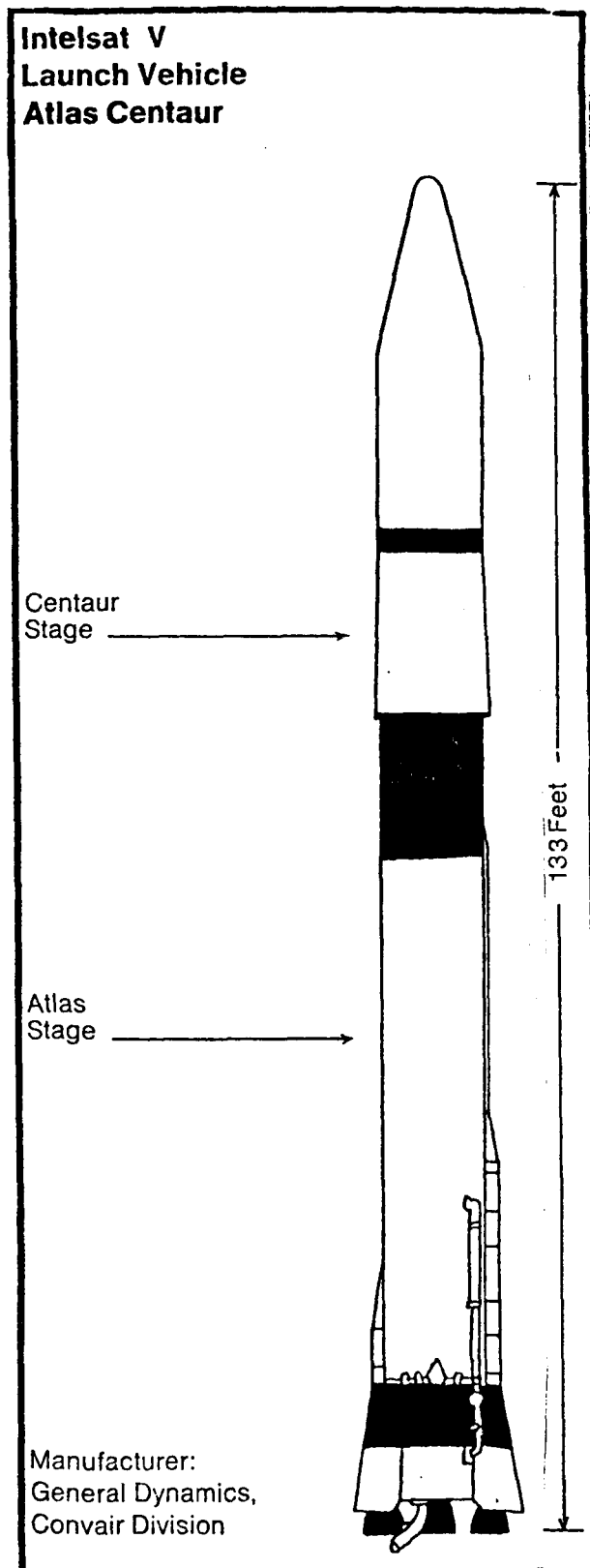
### Propulsion

The propulsion subsystem, excluding the apogee motor, is based on conventional catalytic hydrazine thrusters for transfer orbit and normal geostationary operations. North-south stationkeeping is accomplished by electrothermal hydrazine thrusters which are more efficient than catalytic thrusters. As a result, approximately 30 kg (66 lb.) less hydrazine fuel is required for the mission. The electrothermal units are backed up by conventional catalytic thrusters.

### Electric Power

Electric power for the spacecraft is derived from two wing-like structures that fold out from the main body. These wings are covered on one side with silicon solar cells which convert sunlight into electrical energy. Once extended, the arrays rotate to face the Sun and will thereafter track the Sun providing 1742

watts at the beginning of life. This output will gradually degrade to 1241 watts at the end of several years in orbit. Twice per year the spacecraft will experience a series of passes through the Earth's shadow. At these times the power subsystem is supported by two rechargeable batteries. Early spacecraft will carry nickel cadmium batteries as have all previous INTELSAT satellites. However, starting with the fifth flight, newly developed nickel hydrogen batteries with enhanced life characteristics will be flown.



#### LAUNCH VEHICLE DESCRIPTION

The Intelsat V-C (F-3) will be launched into a transfer orbit by an Atlas-Centaur launch vehicle (Figure 3).

The rocket combination, standing approximately 41 meters (133 ft) high, consists of an Atlas SLV-3D booster and Centaur D-1A second stage.

The Atlas booster develops 1913 kilonewtons (430,000 lb) of thrust at liftoff using two 828,088 newton (184,841 lb) thrust booster engines, one 267,000 newton (60,000 lb) thrust sustainer engine, and two vernier engines developing 3006 newton (676 lb) thrust each. Its propellants are RP-1 (a kerosene type fuel) and liquid oxygen (LOX).

Centaur was the nation's first high energy, liquid hydrogen-liquid oxygen propelled launch vehicle. Developed and launched under the direction of NASA, Lewis Research Center, Cleveland, Ohio, it became operational in 1966 with the launch of Surveyor 1, the first U.S. spacecraft to soft land on the Moon's surface.

The Centaur stage is being used not only in combination with the Atlas booster, but also in combination with the Titan III booster. The Titan Centaur combination has successfully launched four heavier payloads into interplanetary trajectories. These were two Helios spacecraft towards the Sun and the two Viking spacecraft towards the planet Mars.

Fig. 3

The Centaur stage for the Atlas booster was modernized over 7 years ago and designated D-1A. This modernization consisted primarily of the integrated electronic system controlled by a digital computer. This flight proven "astrionics" system checks itself and all other systems prior to and during the launch phase; during flight it has the prime role of controlling all events after the liftoff. This system is located on the equipment module located on the forward end of the Centaur stage.

The launch vehicle characteristics are contained in Table 2.

**TABLE 2**  
**LAUNCH VEHICLE CHARACTERISTICS**

Liftoff weight including spacecraft	147,871 kg (326,000 lb)
Liftoff Height	40.5 meters (133 ft)
Launch Complex	36 B
Launch Azimuth	97.6 degrees
	<u>Atlas Booster</u> <u>Centaur Stage</u>
Weight	128,934 kg (284,248 lb)      17,676 kg (38,970 lb)
Height	21.3 meters (70 ft)      18.6 meters (61 ft) (with payload fairing)
Thrust	1931 kilonewtons (431,000 lb) (sea level)      1334.4 kilonewtons (30,000 lb) (vacuum)
Propellants	Liquid Oxygen and RP-1      Liquid Oxygen and Liquid Hydrogen
Propulsion	MA-5 system: 2 - 828,088 newton (184,841 lb) thrust engines; 1 - 267,000 newton (60,000 lb) sustainer engine; and 2 - 2982 newton (670 lb) thrust vernier engines      2 - 67,000 newton (15,000 lb) thrust RL-10 engines. 14 small hydrogen peroxide thrusters.
Guidance	Preprogrammed profile through Inertial guidance BECO. Switch to inertial guidance for sustainer phase.

The 16,000 word-capacity computer, which is the heart of the system, replaces the original 4800-word capacity computer and enables it to take over many of the functions previously handled by separate mechanical and electrical systems. The new Centaur system handles navigation, guidance tasks, control pressurization, propellant management, telemetry formats and transmission, and initiation of vehicle events.

Many of the command and control functions previously performed by Atlas systems are now being handled by the Centaur equipment also. Systems which are totally integrated include guidance, flight control, telemetry, and event sequence initiation.

One of the major advantages of the new Centaur D-1A system is the increased flexibility in planning new missions. In the past, hardware frequently had to be modified for each mission. Now most operational needs can be met by changing the computer software.

INTELSAT TEAMINTELSAT

Andrea Caruso	Deputy Director General - Administration
Francis Latapie	Acting Deputy Director General - Administration
Allan M. McCaskill	Manager, Launch Vehicle Program Office

NASA HEADQUARTERS

Stanley I. Weiss	Associate Administrator for Space Transportation Operations
J.B. Mahon	Director, Expendable Launch Vehicles
F.R. Schmidt	Atlas-Centaur Manager

LEWIS RESEARCH CENTER

James E. Patterson	Director, Launch Vehicles
Richard E. Orzechowski	Mission Project Engineer

KENNEDY SPACE CENTER

Charles D. Gay	Director, Expendable Vehicles Operations
Donald G. Sheppard	Chief, Automated Payloads Division
Larry F. Kruse	INTELSAT Spacecraft Coordinator

PRIME CONTRACTORSRESPONSIBILITY

Ford Aerospace & Communications Corporation Palo Alto, CA	INTELSAT V Spacecraft
General Dynamics/Convair San Diego, CA	Atlas-Centaur Vehicle
Honeywell, Aerospace Division St. Petersburg, FL	Centaur Guidance Inertial Measurement Group
Pratt & Whitney West Palm Beach, FL	Centaur RL-10 Engines
Teledyne Systems Co. Northridge, CA	Digital Computer Unit/ PCM Telemetry

1. Report No. NASA CR-135324		2. Government Accession No.		3. Recipient's Catalog No.																	
4. Title and Subtitle QUIET CLEAN SHORT-HAUL EXPERIMENTAL ENGINE (QCSEE) OVER-THE-WING PROPULSION SYSTEM TEST REPORT Volume II - Aerodynamics and Performance				5. Report Date July 1978																	
				6. Performing Organization Code																	
7. Author(s) Advanced Engineering and Technology Programs Department Group Advanced Engineering Division				8. Performing Organization Report No. R77AEG474																	
				10. Work Unit No.																	
9. Performing Organization Name and Address General Electric Company 1 Jimson Road Cincinnati, Ohio 45215				11. Contract or Grant No. NAS3-18021																	
				13. Type of Report and Period Covered Contractor Report																	
12. Sponsoring Agency Name and Address National Aeronautics and Space Administration Washington, D.C. 20546				14. Sponsoring Agency Code																	
15. Supplementary Notes Test Report; Project Manager: C.C. Ciepluch, QCSEE Project Office; Technical Adviser: H.G. Yacobucci, NASA Lewis Research Center, Cleveland, Ohio 44135																					
16. Abstract  The Quiet, Clean, Short-Haul, Experimental Engine (QCSEE) Program includes the design and testing of high-bypass, geared-turbofan engines, with nacelles, forming the propulsion systems for short-haul, passenger aircraft. These systems contain the technology required for externally blown-flap-type aircraft for introduction into passenger service in the 1980's.  This report covers sea-level, static, ground testing of the Over-the-Wing (OTW) engine and boilerplate nacelle components. The report consists of four volumes and two appendices as follows:  <table border="0" style="width: 100%;"> <tr> <td style="width: 30%;">Volume I</td> <td>Summary Report NASA CR-135323</td> <td rowspan="5" style="vertical-align: middle; font-size: 3em;">}</td> <td rowspan="5" style="vertical-align: middle;">For Government Use Only</td> </tr> <tr> <td>Volume II</td> <td>Aerodynamics and Performance NASA CR-135324</td> </tr> <tr> <td>Volume III</td> <td>Mechanical Performance NASA CR-135325</td> </tr> <tr> <td>Volume IV</td> <td>Acoustic Performance NASA CR-135326</td> </tr> <tr> <td>Volume A</td> <td>Detailed Engine Performance</td> </tr> <tr> <td>Volume B</td> <td>Acoustic Data</td> <td></td> <td></td> </tr> </table>						Volume I	Summary Report NASA CR-135323	}	For Government Use Only	Volume II	Aerodynamics and Performance NASA CR-135324	Volume III	Mechanical Performance NASA CR-135325	Volume IV	Acoustic Performance NASA CR-135326	Volume A	Detailed Engine Performance	Volume B	Acoustic Data		
Volume I	Summary Report NASA CR-135323	}	For Government Use Only																		
Volume II	Aerodynamics and Performance NASA CR-135324																				
Volume III	Mechanical Performance NASA CR-135325																				
Volume IV	Acoustic Performance NASA CR-135326																				
Volume A	Detailed Engine Performance																				
Volume B	Acoustic Data																				
17. Key Words (Suggested by Author(s)) Aircraft Propulsion and Power Integrated Engine/Nacelle Structures Propulsion System Testing																					
19. Security Classif. (of this report) Unclassified		20. Security Classif. (of this page) Unclassified		21. No. of Pages 50																	
				22. Price																	

\* For sale by the National Technical Information Service, Springfield, Virginia 22151



## TABLE OF CONTENTS

<u>Section</u>		<u>Page</u>
1.0	SUMMARY	1
2.0	INTRODUCTION	2
3.0	PROPULSION SYSTEM PERFORMANCE	4
3.1	Performance Objectives	4
3.2	Uninstalled Performance	4
3.2.1	Thrust Versus Airflow	6
3.2.2	Specific Fuel Consumption	9
3.3	Installed Performance	9
3.3.1	Thrust Versus Airflow	9
3.3.2	Specific Fuel Consumption	9
3.4	Turbine Inlet Temperature	9
3.5	Exhaust Velocity	13
3.6	Reverse Mode Thrust	13
4.0	OTW FAN AERODYNAMIC PERFORMANCE	18
4.1	Introduction and Summary	18
4.2	Fan Bypass Region Overall Performance	18
4.3	Fan Hub (Inlet) Region Overall Performance	22
4.4	Fan Bypass Radial Profiles	22
4.5	Fan Hub (Core Inlet) Radial Profiles	23
5.0	"D" NOZZLE AND REVERSER PERFORMANCE	26
5.1	Pretest Performance Predictions	26
5.2	Experimental Results	32
5.2.1	"D" Nozzle Geometric Characteristics	32
5.2.2	"D" Nozzle Flow Coefficients	32
5.2.3	"D" Nozzle Velocity Coefficients	32
5.2.4	Exit Traverse Data	39
5.2.5	Reverser Performance	39
	REFERENCES	43

PRECEDING PAGE BLANK NOT FILMED

## LIST OF ILLUSTRATIONS

<u>Figure</u>		<u>Page</u>
1.	Axial Thrust Component Versus Airflow.	7
2.	Equivalent Conical Nozzle Thrust Versus Airflow - Uninstalled.	8
3.	Specific Fuel Consumption Versus Thrust - Uninstalled.	10
4.	Equivalent Conical Nozzle Thrust Versus Airflow - Installed.	11
5.	Specific Fuel Consumption Versus Thrust - Installed.	12
6.	Exhaust Velocity Versus Airflow.	14
7.	Core Stream Theoretical Exhaust Velocity Versus Airflow.	15
8.	Bypass Stream Theoretical Exhaust Velocity Versus Airflow.	16
9.	Reverse Thrust Versus Airflow.	17
10.	QCSEE OTW Bypass (Tip) Map.	19
11.	QCSEE OTW Core (Hub) Map.	20
12.	Fan Bypass Radial Profiles at Design Speed.	24
13.	Fan Hub (Core) Radial Profiles at Design Speed.	25
14.	"D" Nozzle Geometry.	27
15.	QCSEE OTW Engine "D" Nozzle Estimated Flow Coefficients.	28
16.	QCSEE OTW Engine "D" Nozzle Estimated Axial Velocity Coefficients.	29
17.	QCSEE OTW Engine "D" Nozzle Estimated Exit Area Characteristics.	30
18.	QCSEE OTW Engine "D" Nozzle Estimated Efflux Kickdown Angle.	31
19.	"D" Nozzle Exit Plane Tuft Pattern Orientation.	34
20.	"D" Nozzle Tuft Survey at Idle Power.	35

LIST OF ILLUSTRATIONS (Concluded)

<u>Figure</u>		<u>Page</u>
21.	"D" Nozzle Tuft Survey at 3000 rpm Fan Speed.	36
22.	QCSEE OTW Engine "D" Nozzle Flow Coefficients.	37
23.	QCSEE OTW Engine "D" Nozzle Velocity Coefficients.	38
24.	QCSEE OTW Engine Exit Velocity Profiles.	41

LIST OF TABLES

<u>Table</u>		<u>Page</u>
I.	OTW Propulsion System Performance Requirements.	5
II.	Plotting Symbols for Figures 1 through 9.	6
III.	QCSEE OTW Fan.	18
IV.	Comparison of "D" Nozzle Geometric Characteristics with Predictions.	33
V.	QCSEE OTW Engine Nozzle Exit Traverse Data; Corrected Fan Speed = 91%.	40

## 1.0 SUMMARY

Performance testing of the OTW propulsion system was completed, as scheduled, resulting in the following significant observations.

Forward-thrust performance met contract goals for thrust and sfc with an equivalent conical exhaust nozzle. Uninstalled performance was measured with a bellmouth inlet, and installed performance was measured with a high Mach number inlet. Turbine rotor inlet temperature exceeded objective levels, limiting the ambient temperature to which the engine could be "flat rated."

Fan performance was very good. Airflow exceeded the design intent by 2-3% at high corrected speeds. Bypass efficiency also exceeded the objective level by 0.7 points. Fan hub supercharging was very good, exceeding pressure ratio requirements by 3.4%.

The "D" shaped exhaust nozzle, operating in the forward-thrust mode, had a velocity coefficient about 4 points lower and provided about  $1-1/2^\circ$  more flow turning ( $14^\circ$  compared to  $12-1/2^\circ$ ) than expected from scale-model test results. The latter reduced the axial (measured) thrust component, but may be desirable from a powered-lift standpoint. Although the exhaust nozzle with the side doors in the open (takeoff) position indicated close to the intended area, a larger area might be desirable to increase the airflow through the inlet and achieve greater forward-noise suppression.

Reverse-thrust performance met the contract goal (35% of takeoff thrust) with the blocker angles of  $105^\circ$  and  $115^\circ$  and with a lip length ratio of 0.6. Because of pressure losses in the thrust reverser, the effective exhaust area was somewhat lower than desired, such that the fan operating line was elevated. As a result, the  $115^\circ$  blocker angle caused the fan to approach the stall/instability boundary as evidenced by measured blade stresses. Further reverse testing was done with a blocker angle of  $105^\circ$ . A greater nacelle cross-sectional area would reduce the Mach number entering the exhaust system. This would reduce pressure losses in the reverse mode and permit the objective reverse-thrust level to be reached at lower fan speed, reducing noise levels.

Overall, the initial engine and component performance levels were judged to be quite satisfactory, considering the lack of a scale-model fan test and the constraint of using the same fan cowl hardware as the UTW engine.

## 2.0 INTRODUCTION

The General Electric Company is currently engaged in the Quiet, Clean, Short-haul, Experimental Engine Program (QCSEE) under Contract NAS3-18021 to the NASA-Lewis Research Center. The Over-the-Wing (OTW) experimental engine was designed and built under the program to develop and demonstrate technology applicable to engines for future commercial, short-haul, turbofan aircraft. The initial buildup of the OTW engine and boilerplate nacelle was tested at General Electric's Peebles, Ohio Outdoor Test Site 4D during the period from March 31, 1977 through June 9, 1977.

The "D" shaped OTW exhaust nozzle contained a moveable roof that could be positioned to form a thrust-reverser blocker. The exhaust nozzle was run in the inverted position so that, during reverse-thrust testing, the exhaust gases would be directed downward rather than into the test facility and instrumentation lines.

Initial testing included a mechanical and systems checkout with hard-wall acoustic panels and a bellmouth inlet. Performance data were taken over a range of fan speeds and at three exhaust nozzle areas (side door angles). This phase of testing provided data in the range of takeoff and approach operating conditions to explore "uninstalled" performance with minimum loss of ram recovery. Fan performance characteristics were mapped over a range of fan speeds and operating lines. An acoustic baseline was also run in the unsuppressed, forward-thrust configuration.

The inlet was then changed to the boilerplate high Mach number design to investigate installed performance with real ram-recovery losses. Points were repeated at takeoff and approach operating conditions. Reverse-thrust testing included 105° and 115° blocker angles with a 0.6 lip-length ratio. A reingestion shield, 3.66 m (12 ft) in diameter and 9.14 m (30 ft) long was used to reduce reingestion of hot exhaust gases during reverse-thrust testing, and the effect of this shield on thrust measurements was calibrated in the forward-thrust mode.

Following reverse-thrust performance testing, all hard-wall panels were changed to acoustically treated panels, and an acoustic splitter was added in the fan duct. Fully suppressed acoustic data was taken in the reverse and forward-thrust modes. Additional acoustic tests were then conducted to evaluate the contribution of inlet treatment and the combined effect of the splitter and core exhaust nozzle treatment.

Following the completion of acoustic testing, additional tests were conducted to evaluate control characteristics and engine throttle response in the forward-thrust mode.

The engine was inspected, refurbished, and delivered to NASA-Lewis Research Laboratory on June 30, 1977 for further planned testing adjacent to a wing section.

This volume of the propulsion system test report includes overall propulsion system performance observations and the results of detailed analysis of performance of the fan and of the "D" shaped exhaust nozzle.

### 3.0 PROPULSION SYSTEM PERFORMANCE

#### 3.1 PERFORMANCE OBJECTIVES

The OTW propulsion system was sized for a 93.4-kN (21,000 lbf) thrust, uninstalled, bare engine. It is flat rated to a 305 K (90° F) day. The performance objective levels, as identified in the Statement-of-Work for sea level static operation, are shown in Table I. Also included in Table I are predicted performance for the nominal, experimental engine and corresponding experimental engine results based on testing.

It was predicted that the nominal, experimental engine would exceed objective turbine temperature limits. This was expected as a result of the cycle deck update, which included revision of the core engine characteristics to match the most recent YF101 representations.

The thrust levels shown in Table I for the experimental engine (493-001/1) are the equivalent thrust the engine would have had if a symmetrical, conical, exhaust nozzle were installed. The equivalent-conical-nozzle thrust is based on the measured pressure, temperature, and flow at fan discharge and turbine frame discharge. Appropriate duct losses and mixing losses are included, and the final thrust level is determined based on assumed mixing effectiveness and velocity coefficient.

Engine test results showed that fan flow tended to be higher than predicted. The fan hub produced higher pressure ratio and efficiency than predicted, as discussed in Section 4. Turbine inlet temperature was above predictions primarily due to lower core flow and turbine efficiencies lower than predicted.

#### 3.2 UNINSTALLED PERFORMANCE

As shown in Table I, on a 305 K (90° F) day at sea level static, uninstalled, the experimental engine met the specific fuel consumption (sfc) goal. The turbine inlet temperature (T41) level exceeded the objective by 38 K (69° F). The sfc goal was also met on a standard day, with the T41 level 20 K (36° F) lower than the objective level.

The performance levels for the experimental engine shown in Table I are based on extrapolation from the ambient test conditions at the Peebles test site. The test reading closest to matching the objective, takeoff, performance point had an equivalent conical nozzle thrust of 93.7 kN (21,069 lbf) at 406.6 kg/sec (896.5 lbm/sec) flow. This reading was adjusted for the change in ambient conditions, flow, and thrust level to arrive at the values shown in Table I.



Table I. OTW Propulsion System Performance Requirements.

	Uninstalled			Installed		
	Statement of Work	Nominal Experimental Engine	OTW Engine 493-001/1	Statement of Work	Nominal Experimental Engine	OTW Engine 493-001/1
Takeoff, SLS, 305 K (90° F) Day						
Net Thrust, kN (lbf)	93.4(21000)	93.4(21000)	93.4(21000)	90.3(20300)	90.3(20300)	90.3(20300)
sfc, g/sec-N (lbm/hr-lbf)	0.01019(0.36)	0.00962(0.34)	0.00991(0.35)		0.00991(0.35)	0.01019(0.36)
Turbine Inlet Temperature Increment, * K (° F)	0 (0)	12 (22)	38 (68)		3 (5)	27 (48)
Bypass Ratio - Approximate	10.2	10.3	10.3		10.3	10.3
Cycle Pressure Ratio - Approximate	15.5	16.9	17.2		16.8	17.2
Takeoff, SLS, Standard Day						
Net Thrust, kN (lbf)	93.4(21000)	93.4(21000)	93.4(21000)			
sfc, g/sec-N (lbm/hr-lbf)	0.00991(0.35)	0.00906(0.32)	0.00962(0.34)			
Turbine Inlet Temperature Increment, * K (° F)	0 (0)	-46 (-82)	-20 (-36)			
*Relative to Objective Level	NOTE: Parameters Enclosed in Boxes are Specific Requirements					

### 3.2.1 Thrust Versus Airflow

Thrust/airflow characteristics for the measured thrust are shown in Figure 1. (The plotting symbols used for the performance plots in Figures 1 through 9 are shown in Table II.) The thrust values in Figure 1 are the axial component as measured by the load cell. This differs from engine total thrust by the cosine of the nozzle efflux angle (see Section 5). For comparison, the predicted trends based on the original, scale-model, nozzle trends are included in Figure 1. Observations made during engine test indicated that the efflux angle is about  $1.7^\circ$  higher than the scale model, which would decrease the predicted axial thrust component about 0.5 percent at  $1.58 \text{ m}^2$  ( $2444 \text{ in.}^2$  exhaust nozzle area (A8) and about 0.7 percent at  $1.90 \text{ m}^2$  ( $2947 \text{ in.}^2$ ). Allowing for these differences, the measured engine thrust in the region of  $89.0 \text{ kN}$  ( $20,000 \text{ lbf}$ ) varied from 5.5 percent below the prediction at  $1.58 \text{ m}^2$  ( $2444 \text{ in.}^2$ ) to 3.7 percent below at  $1.90 \text{ m}^2$  ( $2947 \text{ in.}^2$ ).

The equivalent-conical-nozzle thrusts for the forward-mode test are shown in Figure 2. This is the thrust that would result from the measured temperature, pressure, and flow of the core and bypass streams if they were exhausted through a conical nozzle having a 0.995 velocity coefficient. The nozzle throat area would be variable for the points shown in Figure 2. The demonstrated takeoff operating point occurred at a nozzle area larger than predicted for the engine buildup,  $1.90 \text{ m}^2$  ( $2947 \text{ in.}^2$ ) versus  $1.80 \text{ m}^2$  ( $2783 \text{ in.}^2$ ). The side-door settings required to set the larger area also cause operation at a slightly higher efflux angle than was initially predicted (as discussed in Section 5).

Table II. Plotting Symbols for Figures 1 Through 9.

○	Bellmouth
□	Inlet
◇	Inlet and Shield
△	Reverse
●	$0^\circ$ Door Angle, $1.58 \text{ m}^2$ ( $2444 \text{ in.}^2$ )
◐	$11\text{-}1/2^\circ$ Door Angle, $1.65 \text{ m}^2$ ( $2550 \text{ in.}^2$ )
○	$25^\circ$ Door Angle, $1.80 \text{ m}^2$ ( $2783 \text{ in.}^2$ )
▲	$115^\circ$ Blocker Door Angle
△	$105^\circ$ Blocker Door Angle

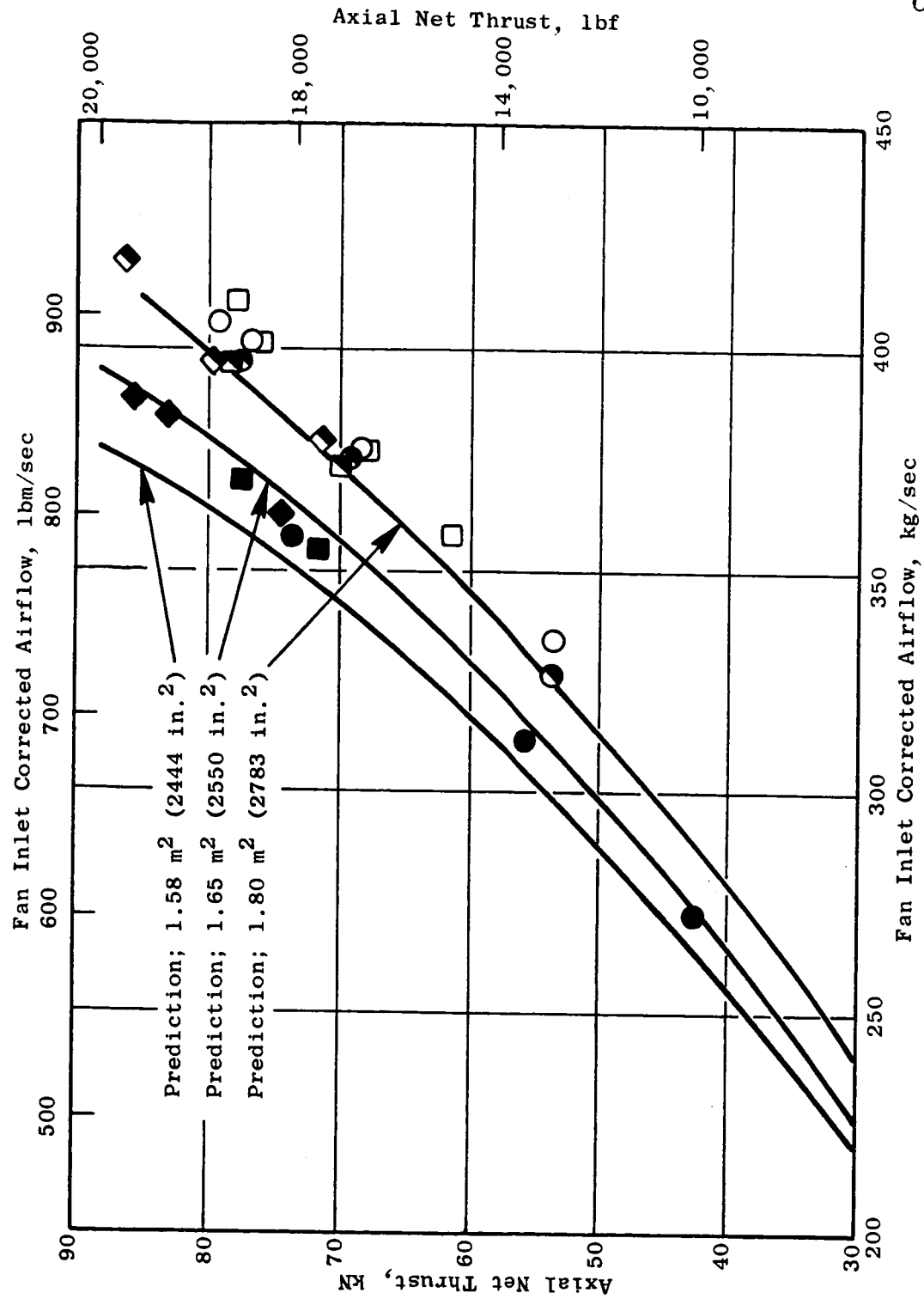


Figure 1. Axial Thrust Component versus Airflow.

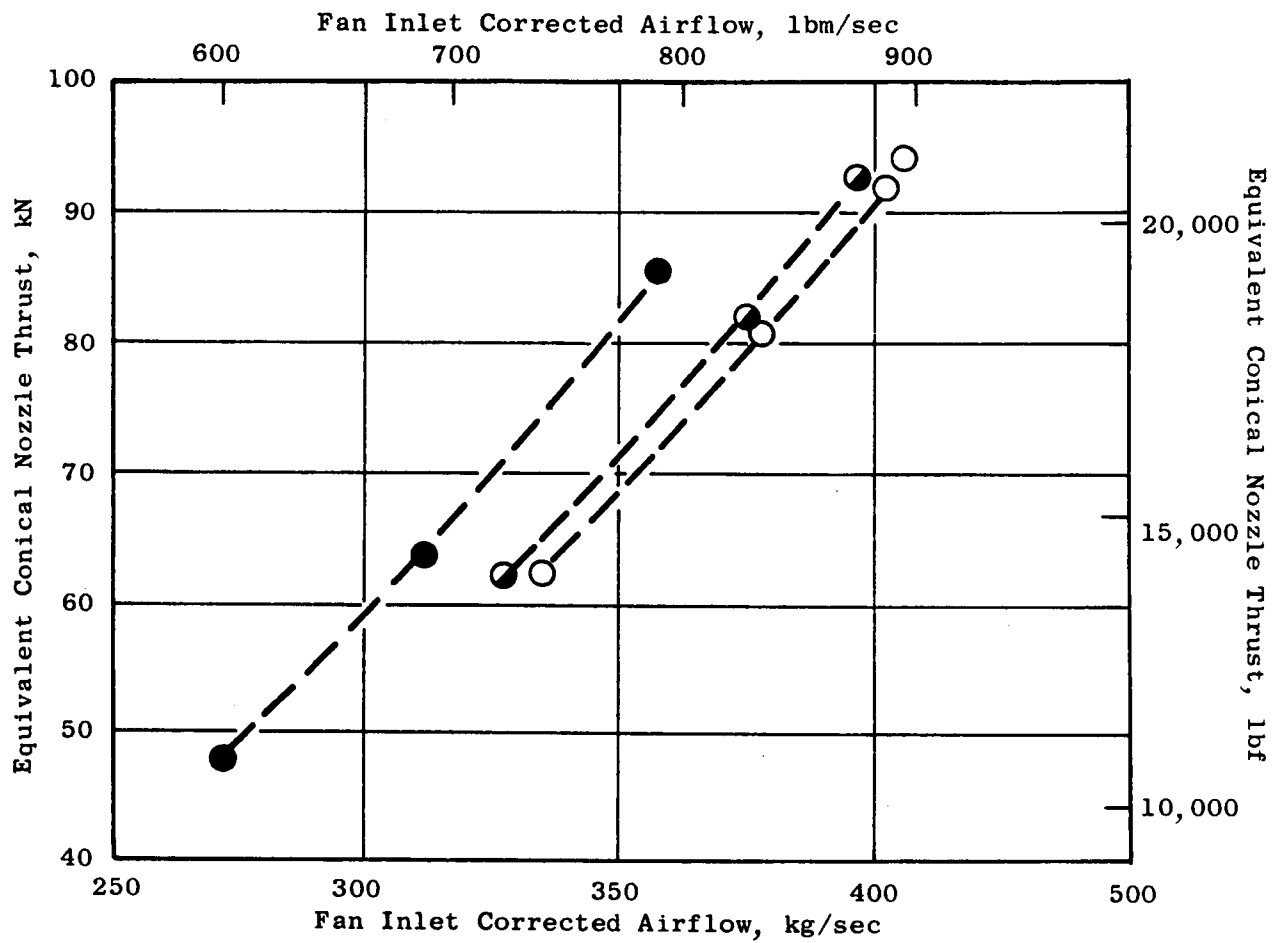


Figure 2. Equivalent Conical Nozzle Thrust versus Airflow - Uninstalled.

### 3.2.2 Specific Fuel Consumption

Specific fuel consumption was about 0.425 mg/sec-N (0.015 lbm/hr-lbf) higher than predicted for the equivalent-conical-nozzle thrust. The sfc trends for the bellmouth runs are shown in Figure 3. At takeoff thrust the sfc is 9.65 mg/sec-N (0.341 lbm/hr-lbf).

### 3.3 INSTALLED PERFORMANCE

The installed thrust objective was 90.3 kN (20,300 lbf) equivalent-conical-nozzle thrust. There were no installed sfc or T41 objectives. The reading which came closest to demonstrating the objective installed takeoff match point had an installed equivalent-conical-nozzle thrust of 90.0 kN (20,288 lbf), at a corrected airflow of 401.2 kg/sec (884.5 lb/sec).

The only loss factor affecting installation is ram recovery. There are no drag terms associated with installed performance.

#### 3.3.1 Thrust Versus Airflow

Installed thrust/airflow characteristics are shown in Figure 4. At the largest nozzle area set during the test, 1.90 m<sup>2</sup> (2947 in.<sup>2</sup>), the thrust/airflow trend was still above the desired level. At 405.5 kg/sec (894 lb/sec) the thrust would have been 91.6 kN (20,600 lbf) at the test nozzle-area setting. The nozzle area would have to be increased about 645 cm<sup>2</sup> (100 in.<sup>2</sup>), based on extrapolations of the test data, to get 90.3 kN (20,300 lbf) installed thrust at 405.5 kg/sec (894 lb/sec) flow.

#### 3.3.2 Specific Fuel Consumption

In the high power regions that test data tend to show sfc about 0.48 mg/sec-N (0.02 lbm/hr-lbf) higher than the predicted equivalent-conical-nozzle trend at takeoff exhaust area. Installed specific fuel consumption is shown in Figure 5. For the test reading at 90.0 kN (20,228 lbf) thrust the sfc is 9.65 mg/sec-N (0.341 lbm/hr-lbf). Extrapolation of this case to a larger nozzle area indicates that a reduction in sfc level of 1 percent would occur at 90.3 kN (20,300 lbf) thrust and 405.5 kg/sec (894 lb/sec) airflow.

### 3.4 TURBINE INLET TEMPERATURE

Turbine inlet temperature tended to run higher than predicted at large nozzle areas. At the cruise area, 1.58 m<sup>2</sup> (2444 in.<sup>2</sup>), the temperature was close to the predicted level at high thrust.

At takeoff thrust (uninstalled) on a hot day, the turbine inlet temperature exceeded the nominal value predicted for the engine buildup by 26 K

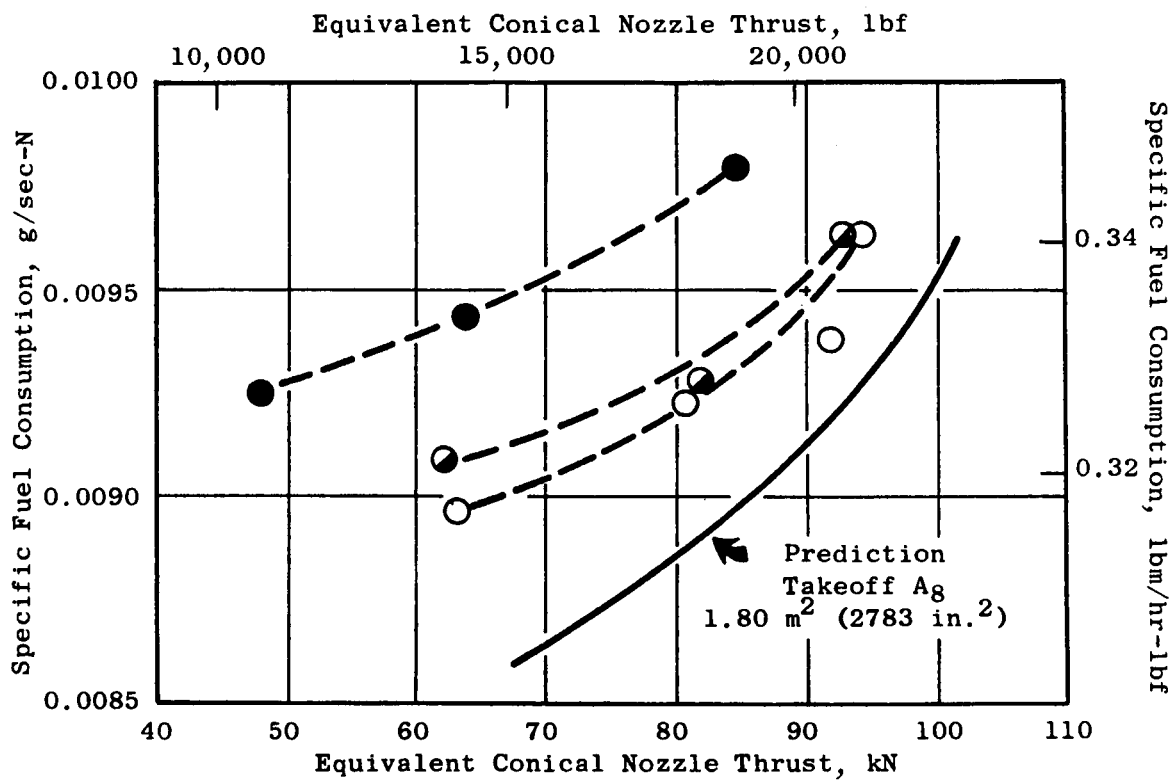


Figure 3. Specific Fuel Consumption versus Thrust - Uninstalled.

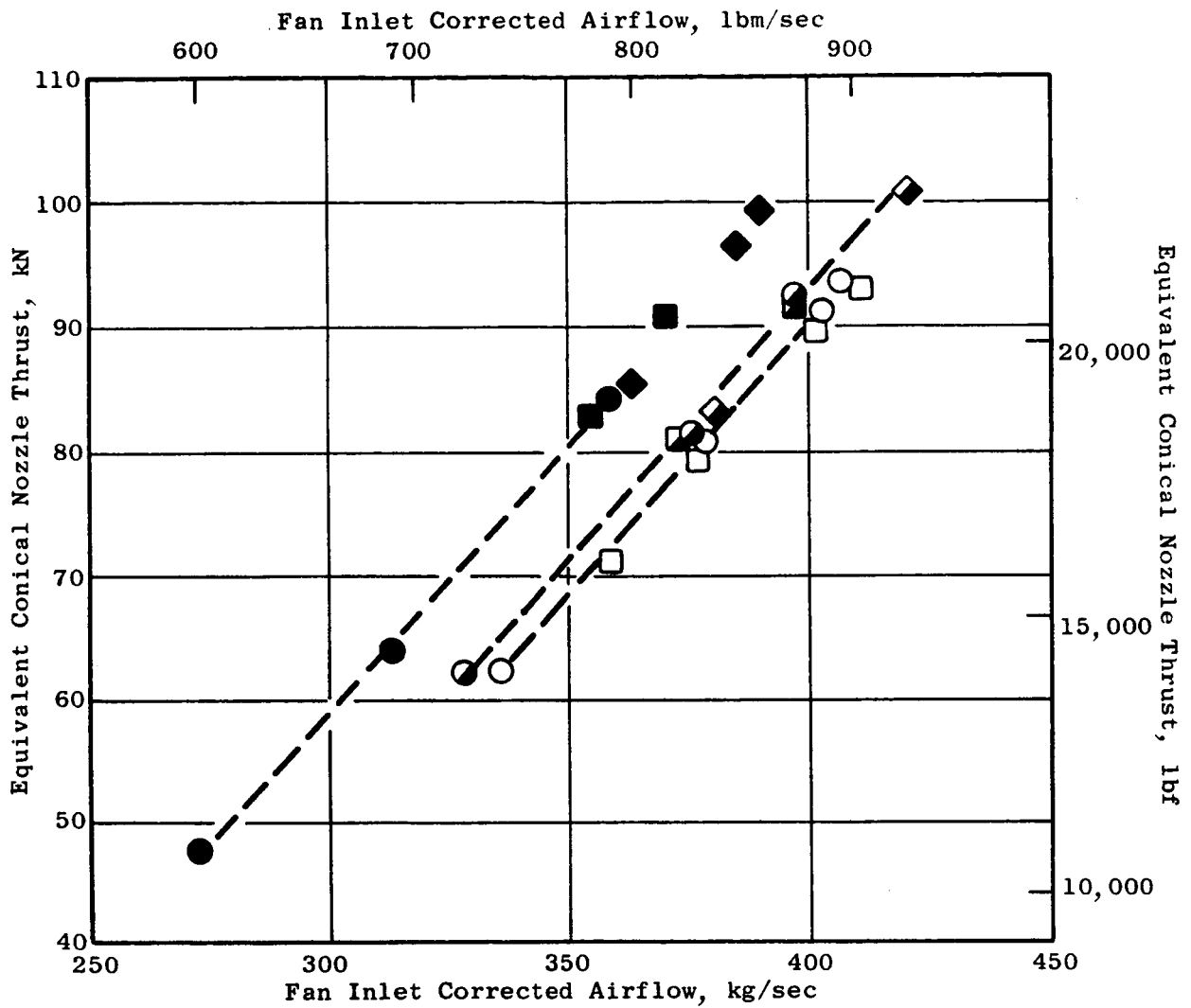


Figure 4. Equivalent Conical Nozzle Thrust versus Airflow - Installed.

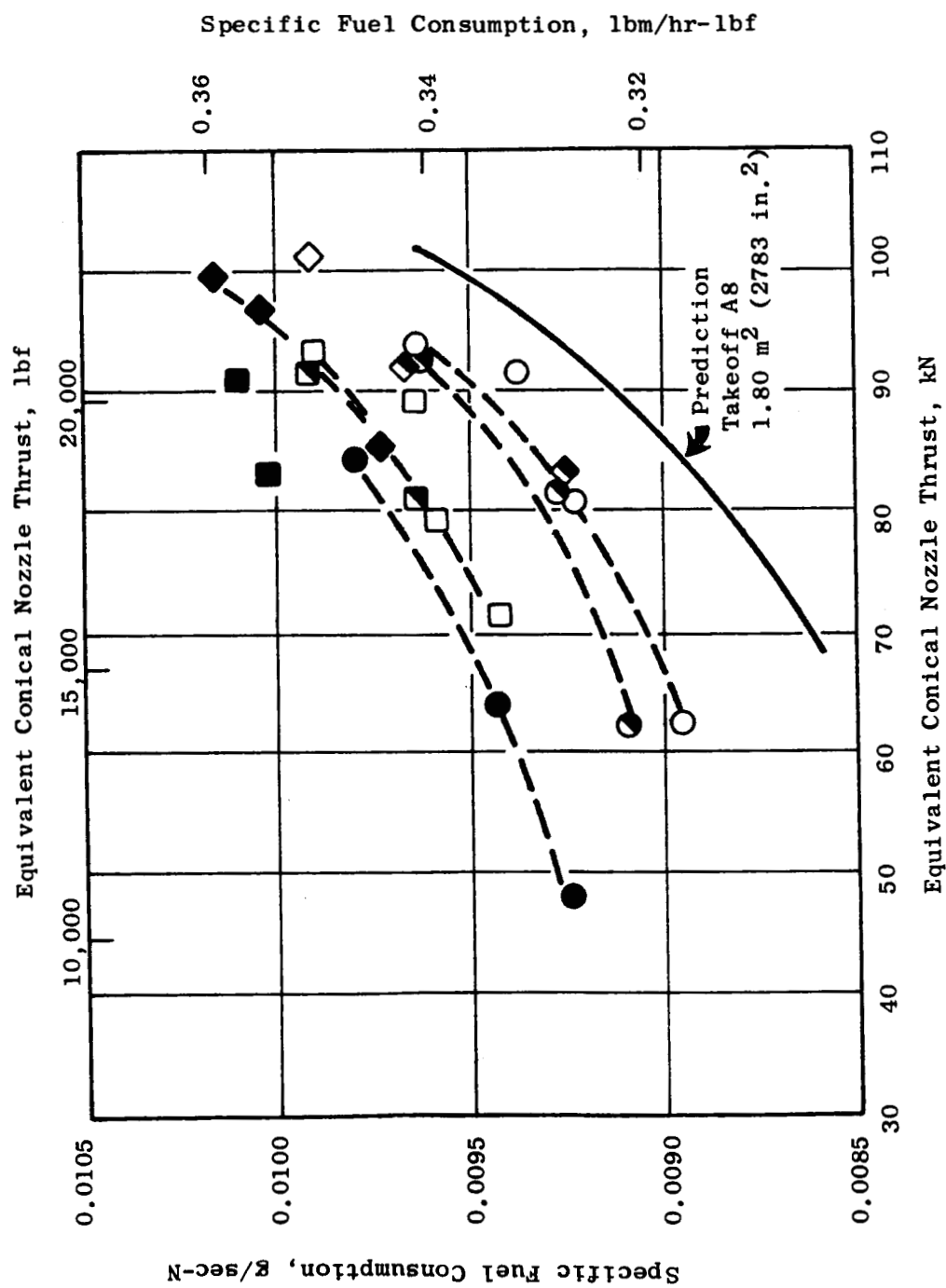


Figure 5. Specific Fuel Consumption versus Thrust - Installed.



(46° F) and exceeded the objective level determined at the time initial engine requirements were established by 38 K (68° F). The temperature level installed was 11 K (20° F) lower than the uninstalled value. On a standard day the turbine inlet temperature was below the objective level primarily because of the inconsistency in objective level definition.

### 3.5 EXHAUST VELOCITY

The corrected exhaust velocity versus airflow is shown in Figure 6. This velocity is based on the mass-average temperature of the bypass and core streams and includes effects of duct losses and mixing losses on pressure. The velocity coefficient is not included in the values shown.

The theoretical core stream velocity (if the core exhausted separately) is shown in figure 7. The pressure loss assumptions for the velocities shown in Figure 7 are assumed to be the same as those for the actual, mixed-flow condition including the pressure drop due to mixing.

The corresponding theoretical bypass stream exhaust velocity is shown in Figure 8. Loss assumptions comparable to the mixed stream was made.

The theoretical velocities establish the upper and lower limits that might be present in the actual, two-dimensional, exhaust stream. The extent of mixing was not established reliably from the test data.

### 3.6 REVERSE MODE THRUST

The reverse mode thrust objective was 35 percent of takeoff thrust, -31.6 kN (-7105 lbf). The reverse-thrust component in the axial direction as measured by the load cell is shown in Figure 9. Thrust in excess of the objective levels was demonstrated for two different blocker door settings, 105° and 115°. At the 115° blocker door angle it was also necessary to open the side doors to provide more exhaust area because stress levels on the fan blading would otherwise have been too high. The reingestion shield was installed in front of the inlet for the reverse mode tests.

At a 105° blocker door angle the objective reverse-thrust level was achieved at 299 kg/sec (660 lb/sec) fan flow and 81 percent fan speed. At the 115° blocker door setting (with side doors open) the objective thrust was obtained at 281 kg/sec (620 lb/sec) flow and 81 percent fan speed.

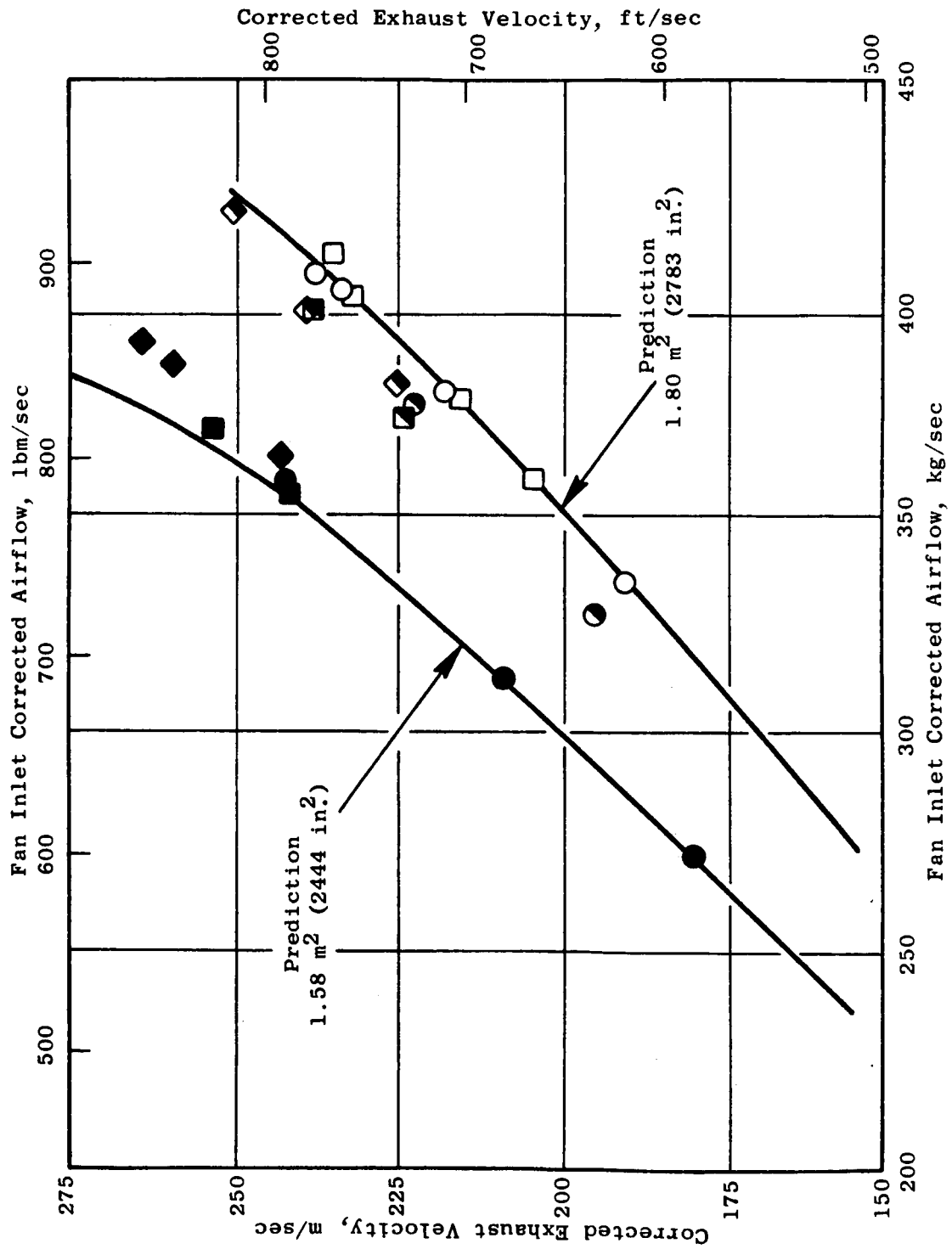


Figure 6. Exhaust Velocity versus Airflow.

ORIGINAL PAGE IS  
OF POOR QUALITY

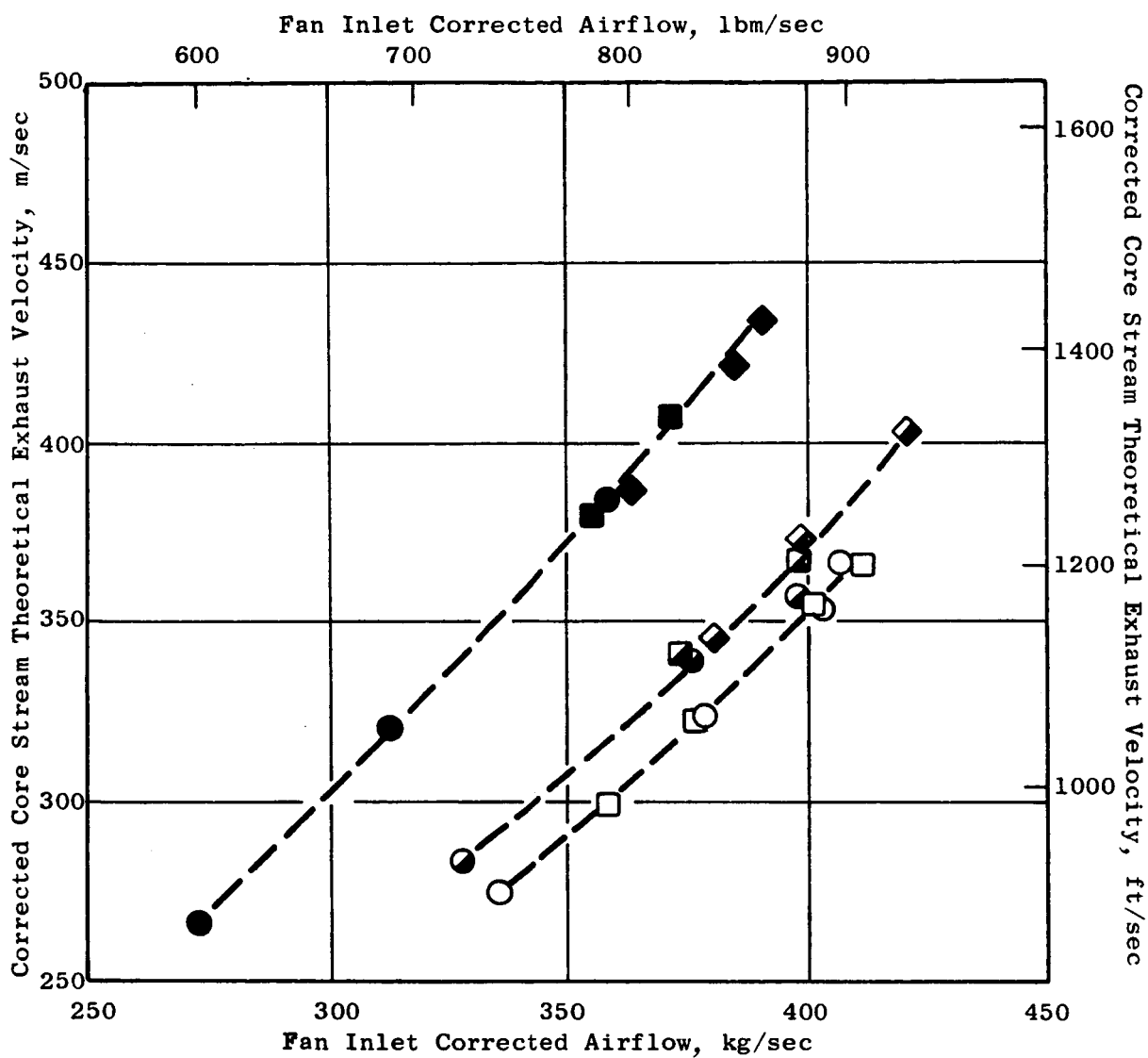


Figure 7. Core Stream Theoretical Exhaust Velocity versus Airflow.

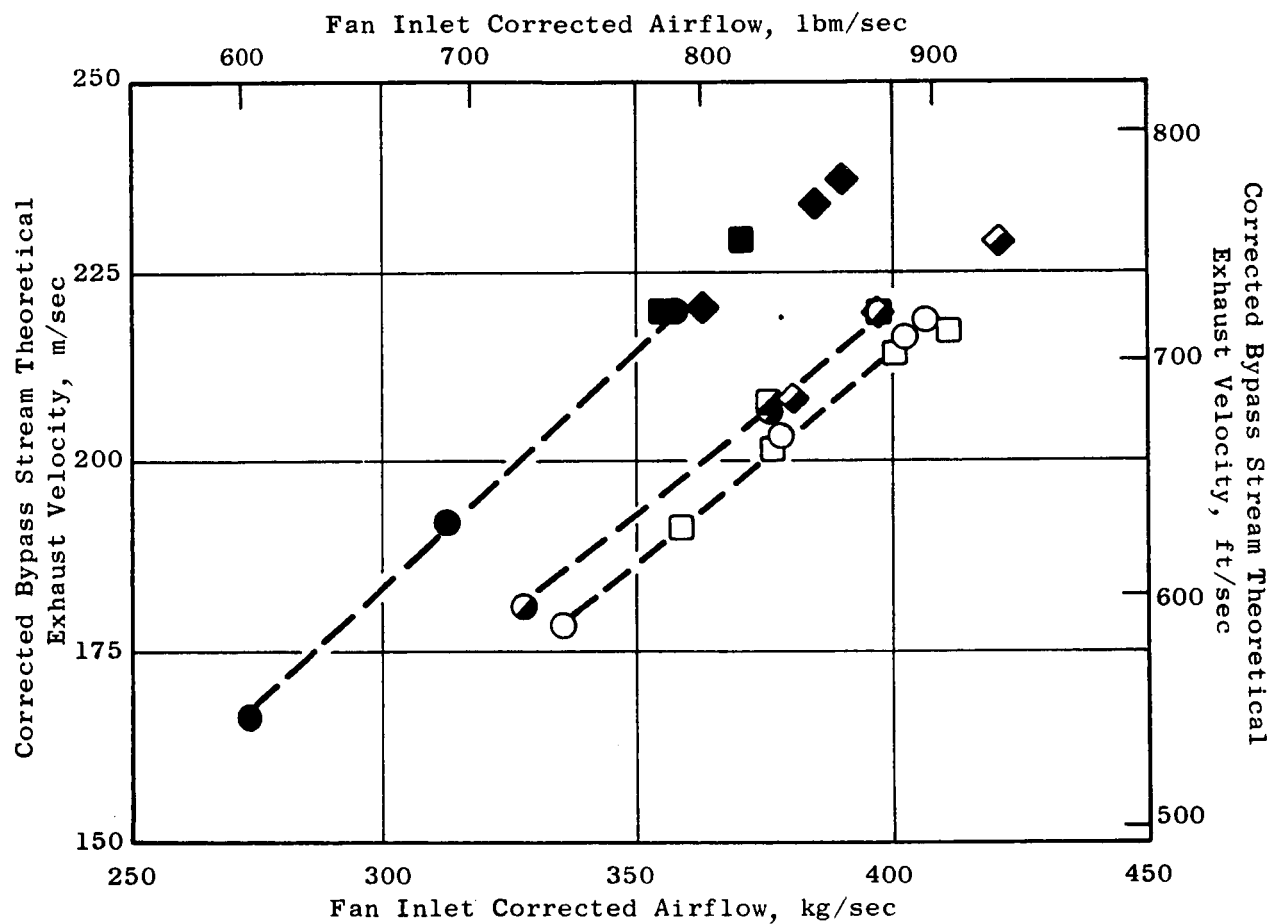


Figure 8. Bypass Stream Theoretical Exhaust Velocity versus Airflow.

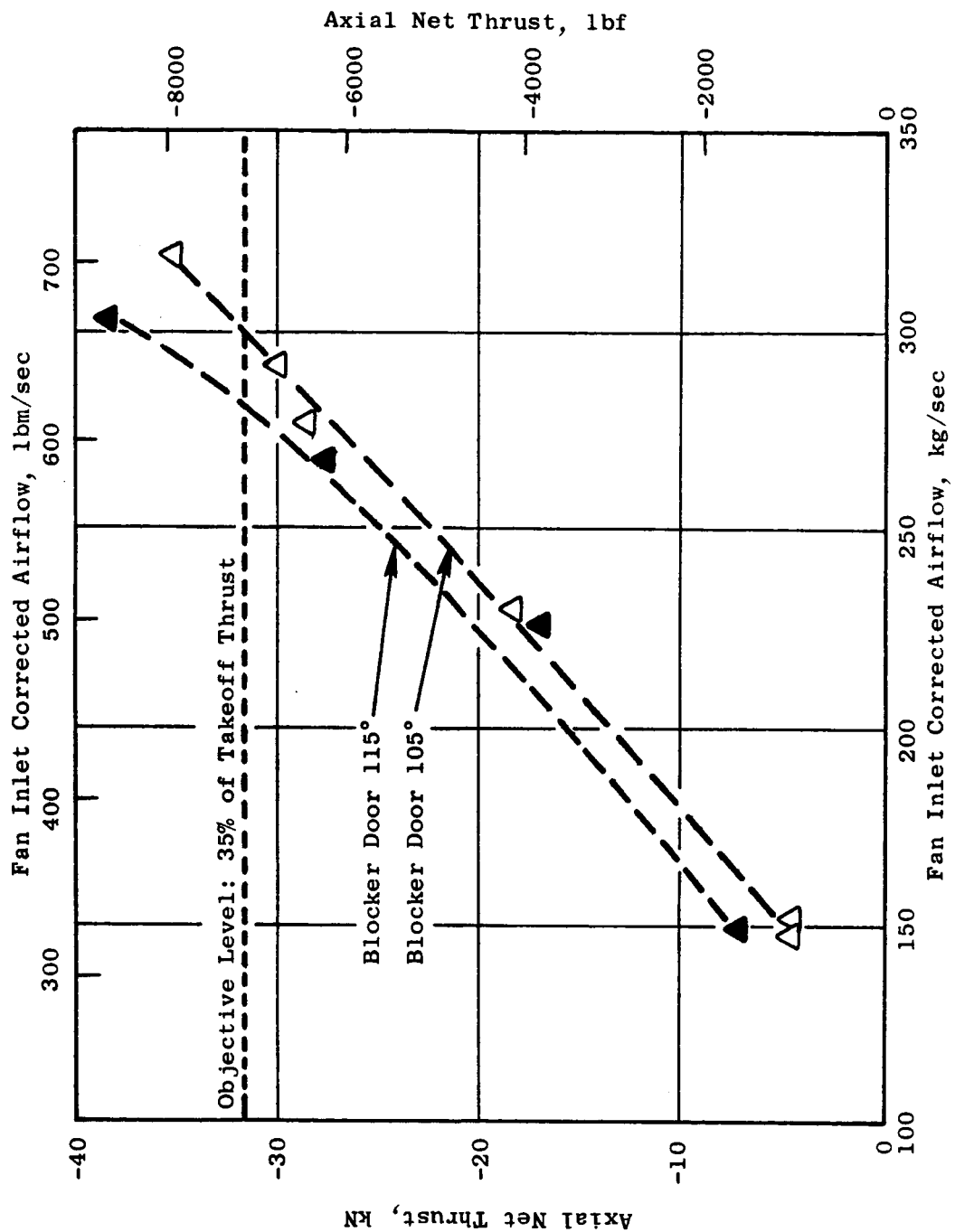


Figure 9. Reverse Thrust versus Airflow.

## 4.0 OTW FAN AERODYNAMIC PERFORMANCE

### 4.1 INTRODUCTION AND SUMMARY

The QCSEE over-the-wing (OTW) engine fan performance was evaluated from test data taken both with a bellmouth inlet and with an accelerating (high Mach) inlet over a range of speeds and nozzle settings. Design-point rotor speed was achieved at one data point (reading 114) where the measured values of fan flow, fan bypass pressure ratio, fan hub (core) pressure ratio, and fan efficiency all exceeded the design-point values. Details of the OTW fan design, both aerodynamic and mechanical, are given in Reference 1. Table III, taken from that report, summarizes the major operating requirements for the fan. Measured performance is presented in Figures 10 and 11 in the form of conventional maps of flow versus pressure ratio both for the bypass and for the hub (core) regions. Although fan stall limits and peak efficiencies were not defined within the extent of available test data, the overall fan performance was judged to satisfy the aerodynamic design criteria.

Table III. QCSEE OTW Fan.

Parameter	Design Point	Takeoff	Maximum Cruise
Total fan flow	408 kg/sec (900 lb/sec)	405.5 kg/sec (894 lb/sec)	405.5 kg/sec (894 lb/sec)
Pressure ratio - bypass flow	1.36	1.34	1.38
Pressure ratio - core flow	1.43	1.43	1.44
Bypass ratio	9.9	10.1	9.8
Corrected tip speed	358 m/sec (1175 ft/sec)	354 m/sec (1162 ft/sec)	359 m/sec (1178 ft/sec)

### 4.2 FAN BYPASS REGION OVERALL PERFORMANCE

Performance characteristics of the fan bypass region are presented in Figure 10. Measured test data points, through which solid lines are drawn, are plotted against background dashed lines which correspond to the fan performance as represented in the engine cycle deck. Although each data point is illustrated by a symbol, indicating a certain percentage of the design-point corrected speed, the data scatter among points of a given symbol was observed to be  $\pm 1\%$  from the indicated speed.

An adjustment to the computed fan flow rates for data taken with the bellmouth inlet (uninstalled), explained in Section 3.2, was incorporated in Figure 10. After this adjustment was made, results similar to those

★ Aerodynamic Design Objective  
 ☆ Demonstrator Engine Objective

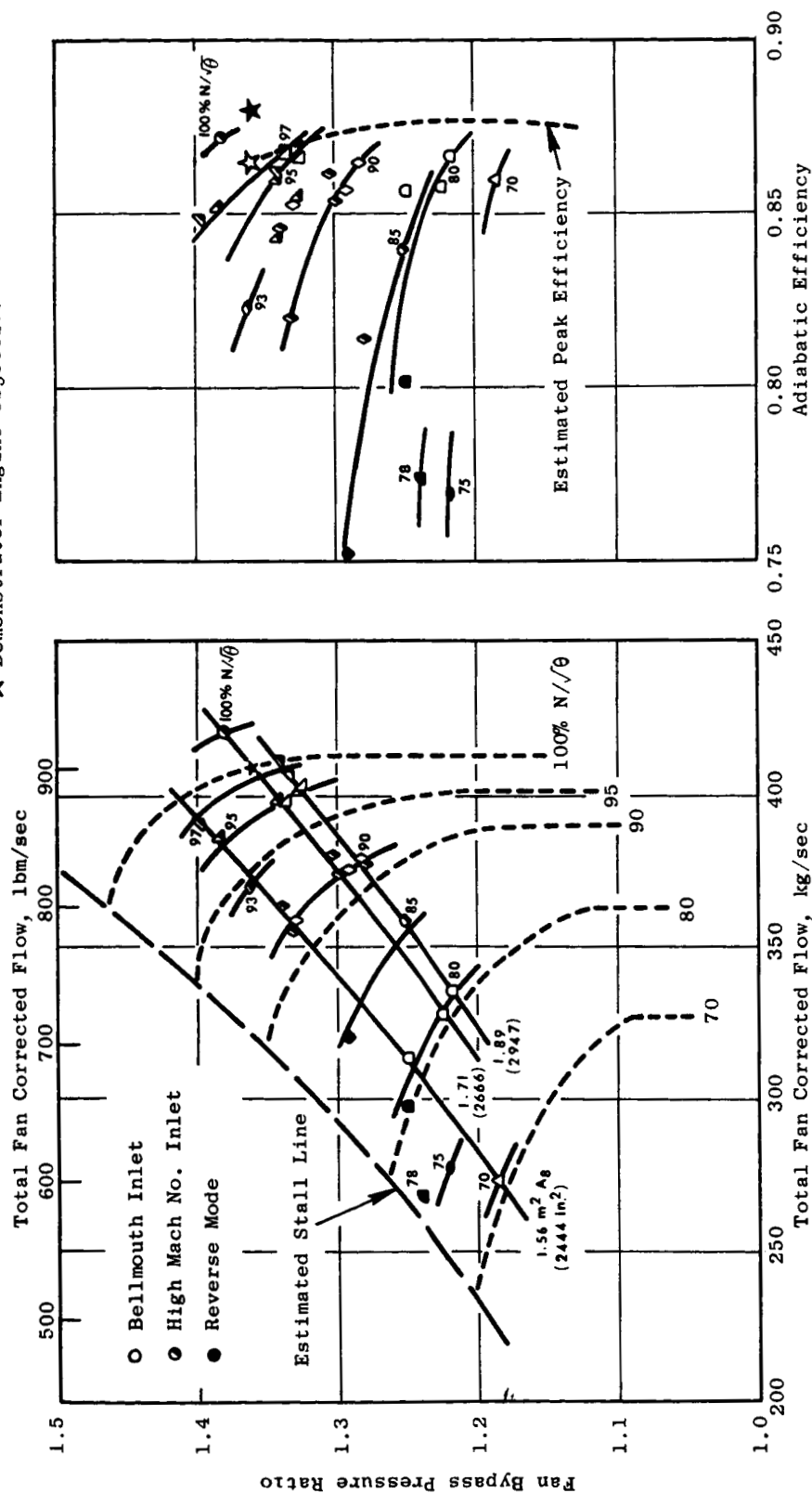


Figure 10. QCSEE OTW Bypass (Tip) Map.

ORIGINAL PAGE IS  
 OF POOR QUALITY

- Bellmouth Inlet
- High Mach No. Inlet
- Reverse Mode
- ★ Aerodynamic Design Objective

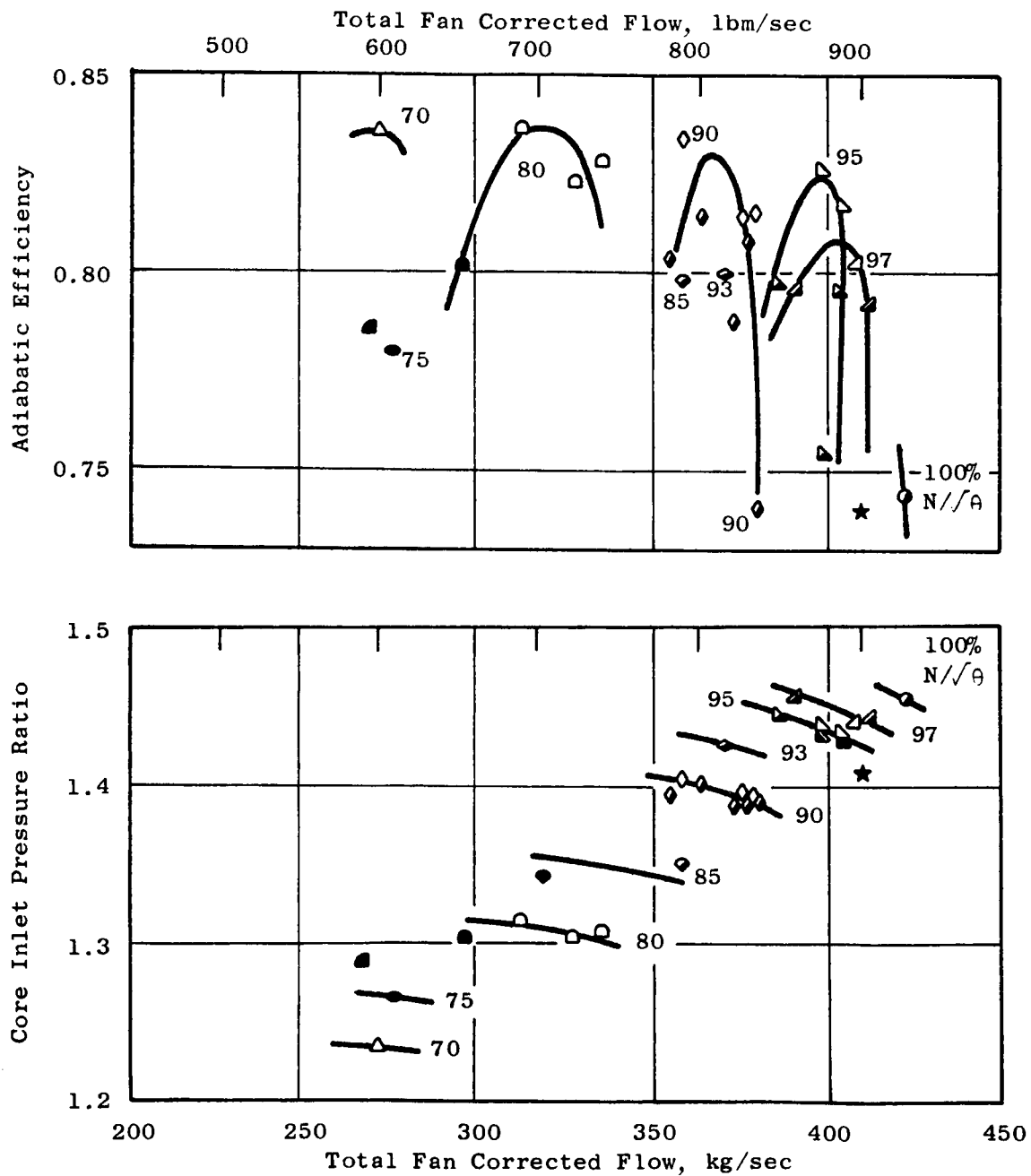


Figure 11. QCSEE OTW Core (Hub) Map.



described in the discussion of fan aerodynamic performance for the UTW engine (Reference 2) were obtained: there were no significant differences in the pumping capability of the OTW fan observed between data taken with the bell-mouth inlet and with the high Mach inlet. Over the speed range tested (85% to 100% of corrected design speed), the measured fan flow exceeded the predicted values by 2-3%. Reading 114, taken at design speed along a fixed-nozzle operating line passing close to the aerodesign point, measured a flow of 420.4 kg/sec (926.8 lbm/sec) and a pressure ratio of 1.382; these were, respectively, 3.0% and 1.6% greater than the design flow of 408.2 kg/sec (900 lbm/sec) and pressure ratio of 1.36.

Fan efficiency is plotted against bypass stream state pressure ratio in Figure 10 and, for comparison, the predicted peak efficiency envelope is also included. The measured data at all speeds exhibit a trend of increasing efficiency as the fan is unthrottled to lower operating lines. Measured peak efficiencies are not distinguishable over the range of nozzle settings tested, and extrapolation of the data would indicate that higher than predicted values of peak efficiency could be achieved along lower than design operating lines. As reported in Reference 1, the predicted fan bypass efficiency at the aerodesign point was 0.88, but an engine derate of 1.5 points lowered the efficiency objective to 0.865 for the demonstrator engine. The measured efficiency for reading 114 was 0.872, which was 0.7 points higher than the objective value for the demonstrator engine but was 0.8 lower than design intent.

Forward-mode data, indicated by the open and the half-filled symbols in Figure 10, were taken primarily in the unthrottled region at high speeds, well below the estimated fan stall line. Reverse-mode data, indicated by the solid symbols in Figure 10, were obtained very close to the estimated stall line but were limited to speeds below 85%. The onset of fan blade instability, not rotating stall, prevented attainment of higher speed data in the reverse mode of operation, as described in the mechanical performance report (Volume III). The major effect of the reverser on fan performance was to raise the operating line, as mentioned in Section 5.2.5. This is illustrated in Figure 10 by comparing the reverse-mode data at 85% and 80% speeds with forward-mode data taken at the same speeds. The fan responded as if being throttled in the conventional sense; the flow and efficiency decreased while the bypass pressure ratio slightly increased. Comparisons of reverse-mode radial profiles of pressure and temperature (as measured by the Plane 15 arc/radial rakes) with those of forward-mode data points of approximately the same speed indicated no performance penalties imposed upon the fan by the reverser except those associated with the higher operating line. The reverse-mode data are thus considered reasonably consistent with the relatively unthrottled forward-mode data and with the engine cycle deck predictions; therefore, the reverse-mode data are used in Figure 10 to expand upon the limited amount of fan performance data taken in the forward mode.

#### 4.3 FAN HUB (CORE INLET) REGION OVERALL PERFORMANCE

Performance characteristics of the fan hub region were measured by radial rakes located in the transition duct, near the core compressor inlet, and are presented in Figure 11. To be consistent with the way in which the fan hub was evaluated in the UTW engine test report (Reference 2), the OTW fan hub pressure ratio and efficiency are plotted against total fan flow. Insufficient data were available to evaluate the efficiency of the fan hub stage separately from the loss of the transition duct, so the data shown in Figure 11 include this loss as accumulated up to Plane 25. At the aerodesign point, design calculations made provisions for an assumed transition duct loss from Plane 21 to Plane 25 of 1.5% ( $P_{21}-P_{25}/P_{21}$ ) which resulted in an adiabatic efficiency loss of 3.4 points.

Shown in Figure 11 for comparison are the aerodesign point values of fan hub pressure ratio of 1.407 and adiabatic efficiency of 0.74 predicted at Plane 25. The measured data of reading 114, taken at design speed along the design fan bypass operating line, indicated a pressure ratio of 1.455 and an efficiency of 0.744. However, this data point was taken in a relatively unthrottled and inefficient region on the fan hub map as shown in Figure 11. As the fan was throttled by closing down the nozzle, the hub efficiency increased significantly and appeared to reach a peak along an operating line near the middle of the nozzle area range tested. At 97% corrected speed, peak efficiency was measured as 0.803, and a peak value of 0.826 was obtained at 95% speed.

The design requirement of high fan hub supercharging was clearly achieved. Even at the unthrottled condition of reading 114, the measured pressure ratio exceeded the design intent by 3.4%. This is significant when considering the high hub loading levels, as indicated by a measured hub work coefficient of 2.8 for reading 114.

#### 4.4 FAN BYPASS RADIAL PROFILES

Radial profiles of total pressure and temperature were determined from data measured with the combination arc/radial rakes located in the fan bypass duct at Plane 15. Fan rotor discharge pressure was determined by circumferential-averaging of the data from radial rake elements positioned between OGV's, and fan stage discharge pressure was obtained from data taken with arc-rake elements spanning a complete OGV passage. The data reduction method used to obtain a specific immersion value of pressure ratio was to divide the arithmetically averaged Plane 15 pressure by the overall average inlet pressure, which included inlet boundary layer rake measurements. The results of this method, though accurate for data taken with the bellmouth inlet, should be cautiously interpreted for data taken with the accelerating high Mach inlet where radial gradients exist near the wall in the inlet pressure profiles at high flows. This method would tend to calculate lower pressure ratios and efficiencies near the outer wall of the accelerating high Mach inlet than would be calculated for identical conditions with the bellmouth inlet.

Figure 12 indicates that the shapes and levels of the measured profiles of reading 114 (recorded with accelerating inlet) are very similar to those of the design intent. Pressure rise is uniformly higher than predicted across the annulus except for a slight drop near the outer wall due in part to the data reduction methods used as explained above. The differences between rotor discharge and stage discharge pressure profiles indicate that bypass OGV losses were close to the design intent. No localized depressions, which would indicate trouble areas, appear in any of the profiles.

#### 4.5 FAN HUB (CORE INLET) RADIAL PROFILES

Radial profiles of total pressure and temperature were determined from data measured with the radial rakes located in the transition duct at Plane 25. Additional data was obtained from several vane-mounted probes at Plane 20. A comparison of the design profiles with those measured by reading 114 is presented in Figure 13; although, as previously noted in Section 4.3, the fan hub performance was generally better than this unthrottled reading would indicate. These profiles define the inlet conditions to the core compressor, with the exclusion of any strut-wake losses generated downstream of Plane 25.

The rotor discharge (Plane 20) pressure and temperature near the inner wall measured significantly higher than expected, perhaps due to the effects of secondary flow as speculated in Reference 1. At Plane 25, however, the pressure and temperature profiles have flattened out to the same shapes as those of the design intent, but at uniformly higher levels across the duct. In the high Mach number environment of the core OGV's, significant losses could be expected as a result of the unexpected OGV inlet profile. The mechanism of the flow deterioration along the end walls is speculated to be a combination of core OGV and transition duct losses, although no instrumentation was available to measure core OGV performance at Plane 21 separately from the duct loss. The net effect, however, did not produce any intolerable distortions or flow limitations to the core compressor.

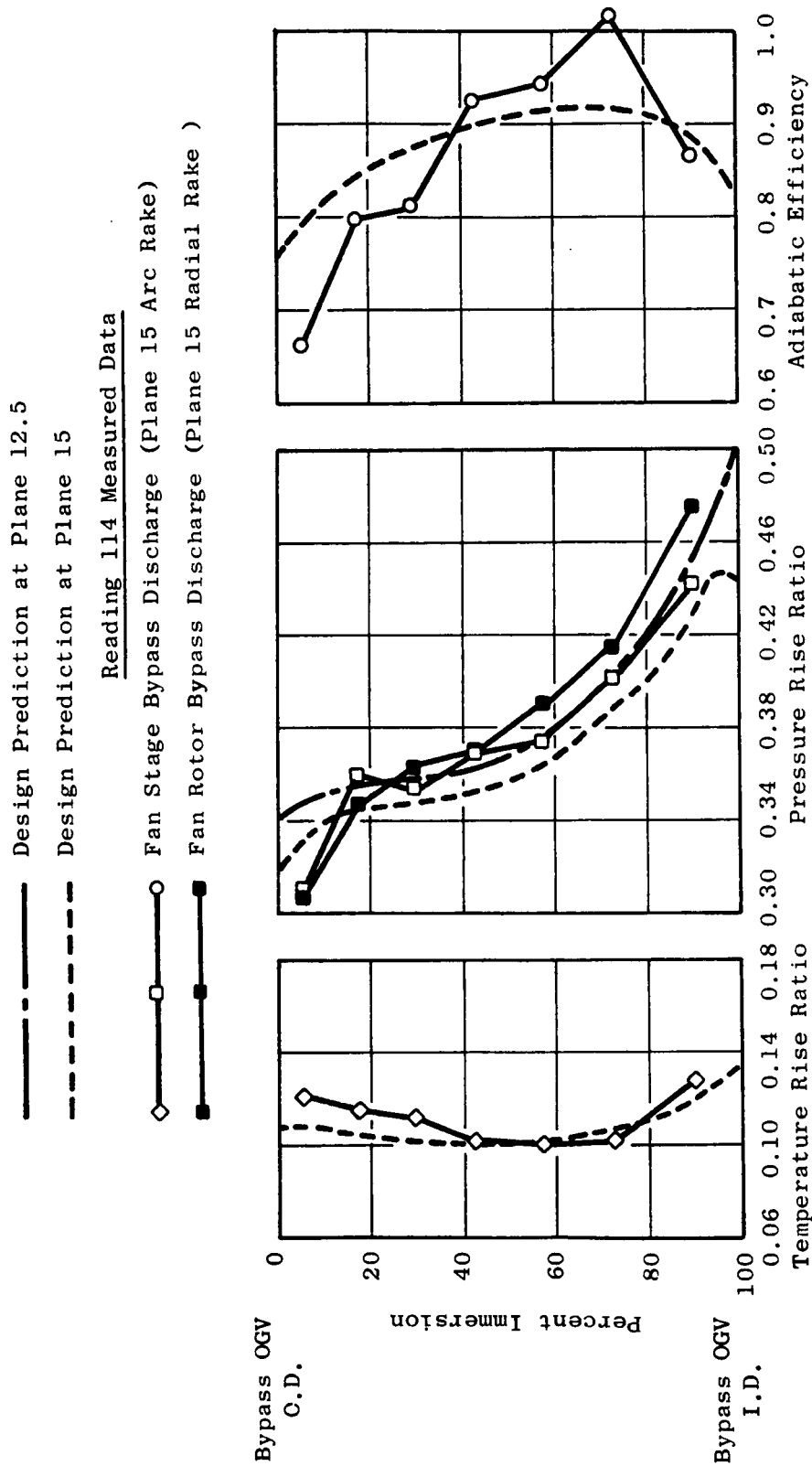


Figure 12. Fan Bypass Radial Profiles at Design Speed.

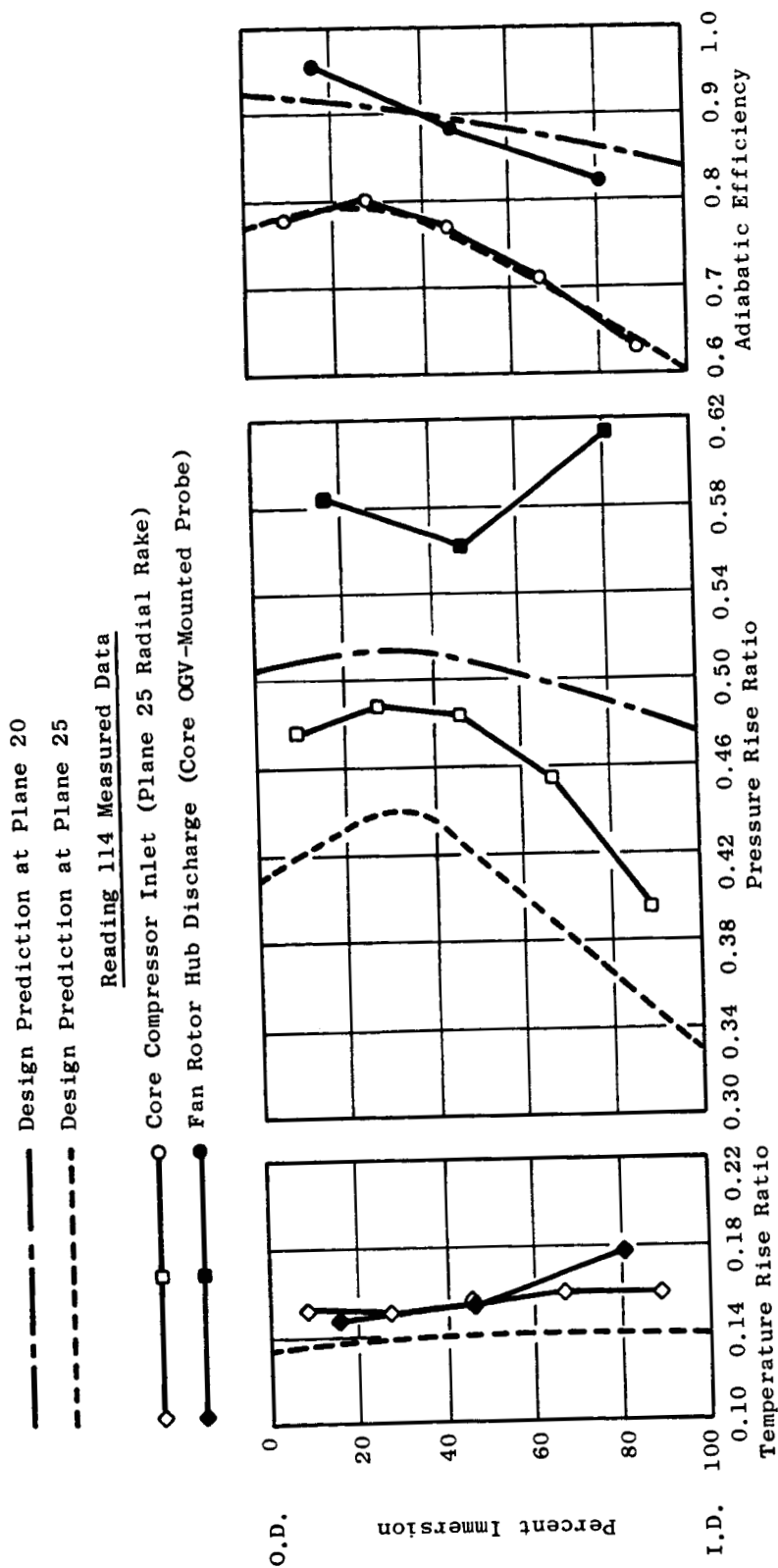


Figure 13. Fan Hub (Core) Radial Profiles at Design Speed.

ORIGINAL PAGE IS  
OF POOR QUALITY

## 5.0 "D" NOZZLE AND REVERSER PERFORMANCE

### 5.1 PRETEST PERFORMANCE PREDICTION

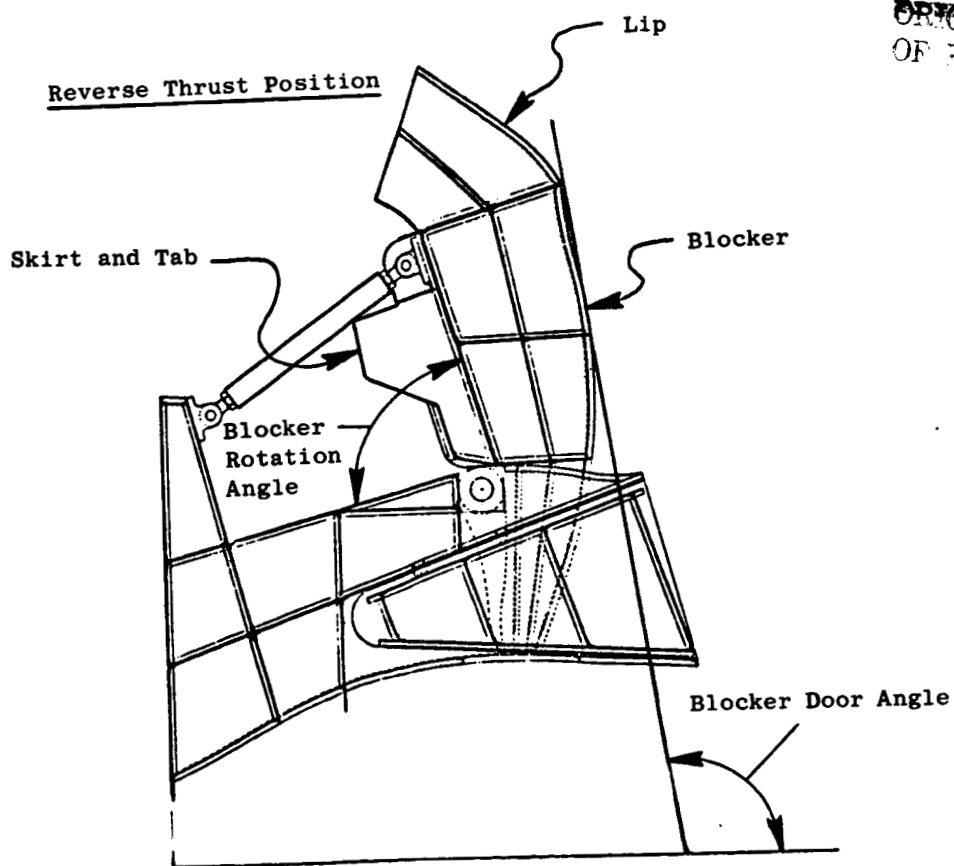
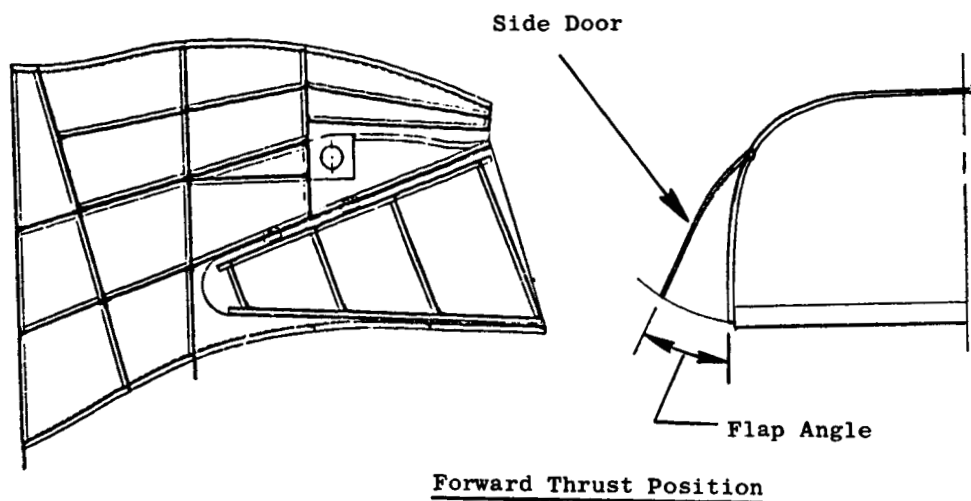
The OTW "D" nozzle and reverser flow paths were developed from scale-model tests at NASA Langley (References 3 and 4). On the basis of experimental results obtained from these tests, nozzle performance characteristics were defined to establish predicted engine performance prior to actual, full-scale testing. The geometry of the nozzle is shown in Figure 14. Figures 15 through 18 show the predicted nozzle performance in terms of nozzle flow coefficient, nozzle axial velocity coefficient, exit area as a function of side door angle, and exhaust nozzle efflux angle as a function of side door angle, respectively. Scale-model, reverser-test results predicted achievement of reverse-thrust goals but with the engine operating in a back-pressured condition because of reduced effective area in reverse.

The predicted flow coefficient characteristics shown in Figure 15 are based upon nozzle exit plane (cycle station 8) flow conditions, consistent with engine cycle bookkeeping methods. Estimated, scale-model, duct-friction, total pressure losses between the scale-model, total pressure measurement plane and the nozzle exit plane were used to convert from pressure-measurement-plane-based model coefficients to full-scale nozzle exit plane equivalent values.

Pretest predictions of nozzle exit plane axial velocity coefficients are given in Figure 16. These data were derived from scale-model data in a manner similar to the flow coefficient data. Additionally the resultant scale-model velocity coefficients were converted to axial coefficients using the measured scale-model efflux kickdown angles reported in References 3 and 4. Conversion to axial values was made to provide a direct comparison with full-scale axial thrust measurements because the Peebles test facility measured only direct force components.

Figure 17 gives the geometric relationship between nozzle side door angle and nozzle exit plane physical area at cross-sectional station 374.4. The shaded region of exit plane shown in Figure 17 represents the cross-sectional area boundary used in preparation of these area characteristics.

Exhaust gas efflux kickdown angle as influenced by nozzle side door setting is given in Figure 18. These data were taken directly from scale-model test results found in References 3 and 4; they represent the deviation from the axial direction along which the resultant full-scale nozzle vector was expected to lie.



ORIGINAL PAGE IS  
OF POOR QUALITY

Figure 14. "D" Nozzle Geometry.

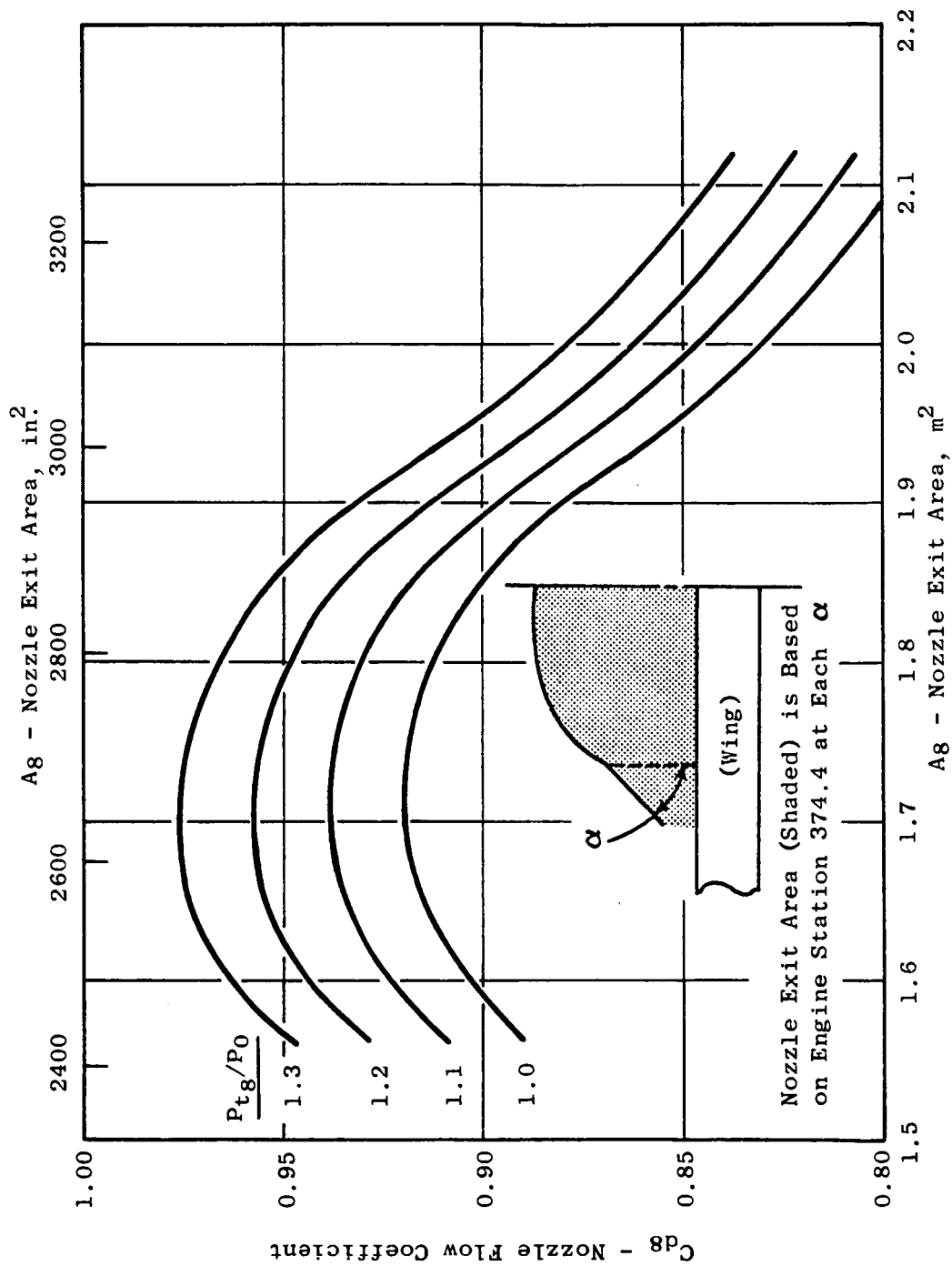


Figure 15. QCSEE OTW Engine "D" Nozzle Estimated Flow Coefficients.



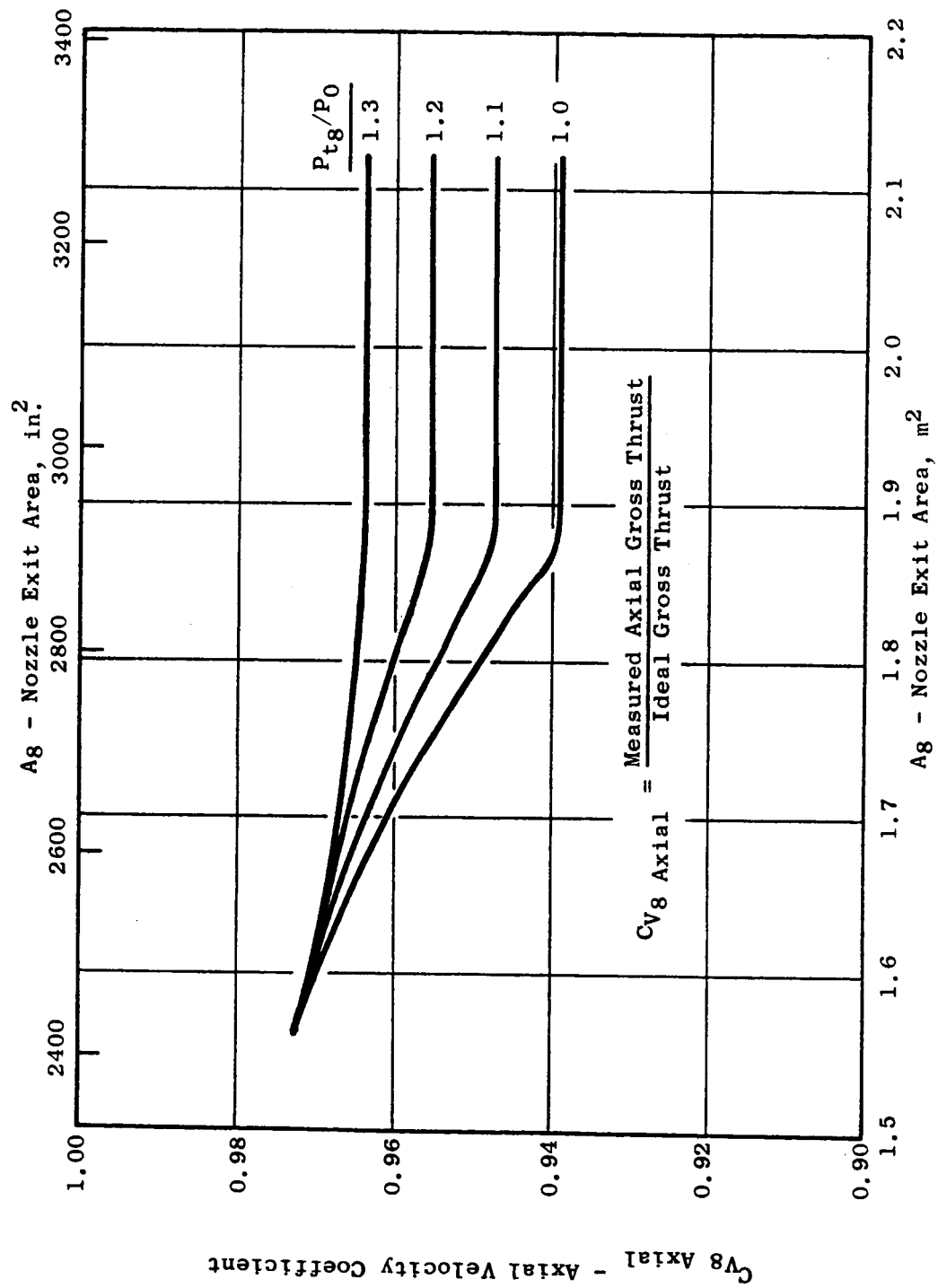


Figure 16. QCSEE OTW Engine "D" Nozzle Estimated Axial Velocity Coefficients.

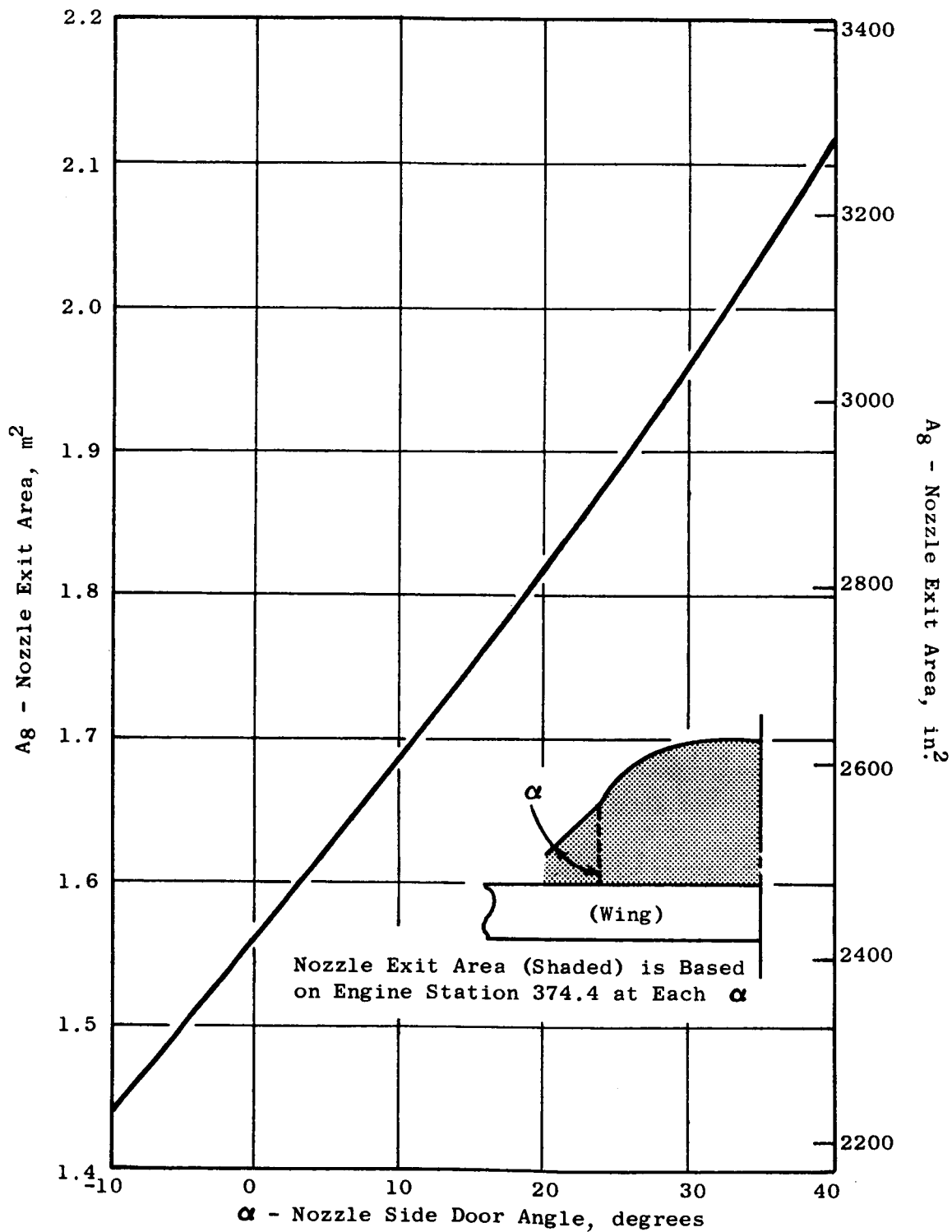


Figure 17. QCSEE OTW Engine "D" Nozzle Estimated Exit Area Characteristics.

ORIGINAL PAGE IS  
OF POOR QUALITY

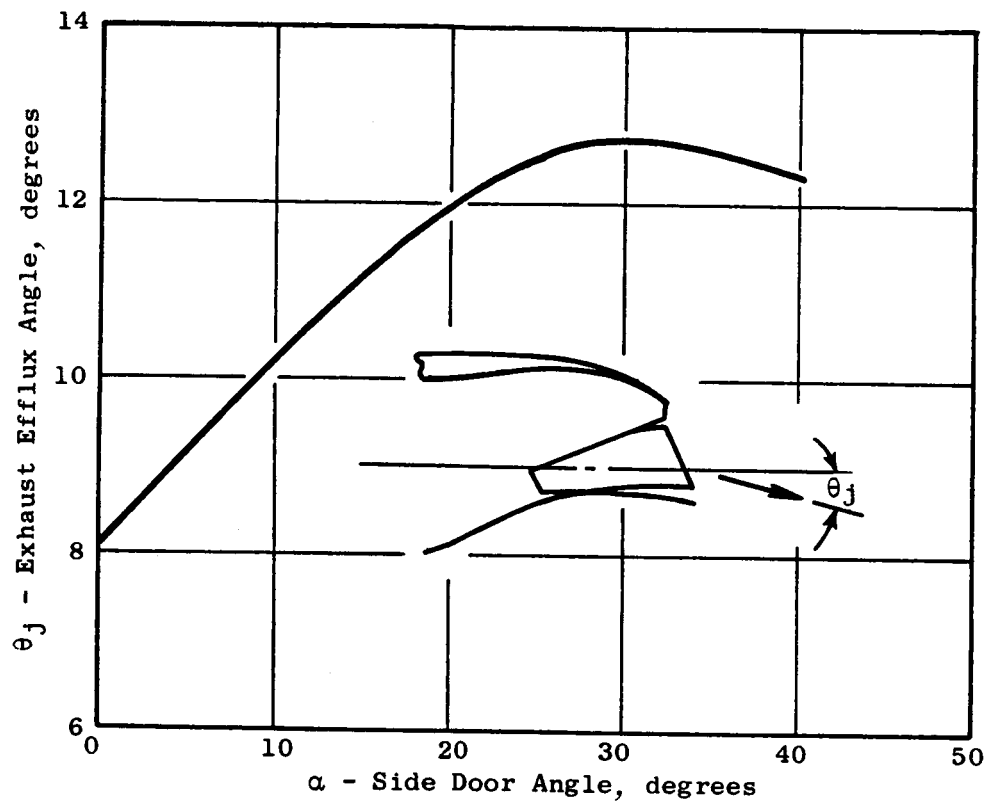


Figure 18. QCSEE OTW Engine "D" Nozzle Estimated Efflux Kickdown Angle.

## 5.2 EXPERIMENTAL RESULTS

### 5.2.1 "D" Nozzle Geometric Characteristics

Measured nozzle geometric characteristics (exit area and kickdown angle) are tabulated on Table IV for comparison with predicted values. The "D" nozzle exit area was measured only at the cruise nozzle area (side door angle setting  $0^\circ$ ) by accurately cutting and measuring a template placed in the nozzle exit plane at engine station 374.4 at ambient conditions. The measured area was determined to be  $1.570 \text{ m}^2$  ( $2433 \text{ in.}^2$ ). With thermal growth allowance at expected engine operating temperatures, this value was adjusted to a "hot" area of  $1.577 \text{ m}^2$  ( $2444 \text{ in.}^2$ ), which is approximately one-percent larger than the nominal design (predicted). Because of the difficulty in accurately measuring the nozzle exit plane at other nozzle side door settings using large templates, area measurements at other side door settings were not made. Rather, the predicted area characteristics versus side door angle were used with a constant area bias adjustment made to reflect the one-percent increase in cruise area relative to design nominal.

The measured nozzle kickdown angles given on Table IV were determined at only one side door angle setting ( $\alpha = 25^\circ$ ) at fan speeds of 3000 rpm and idle. These data, which show full-scale kickdown angles slightly greater than scale-model predictions ( $+ 0.85^\circ$  at idle and  $+ 1.8^\circ$  at 300 rpm) were obtained photographically from tufts as shown on Figure 19, 20, and 21. Kickdown angles for other nozzle areas tested were determined from scale-model predictions biased upward by a constant  $1.80^\circ$  to reflect the  $14.25^\circ$  measured on engine test at the  $25^\circ$  side door setting. These biased angles were then used to establish absolute engine thrust levels from the axial thrust measurements made at Peebles.

### 5.2.2 "D" Nozzle Flow Coefficients

Full-scale nozzle flow coefficient data are compared with scale-model predictions in Figure 22. Average full-scale coefficients are in excellent agreement with predicted values (within one percent) for the three nozzle areas presented.

### 5.2.3 "D" Nozzle Velocity Coefficients

Nozzle absolute (or resultant) velocity coefficients determined from full-scale testing at Peebles are presented in Figure 23. Comparable scale-model predictions are also given for the three nozzle areas investigated during engine tests. The absolute velocity coefficients were determined from axial force readings divided by the cosine of the nozzle efflux kickdown angle. For the scale-model predicted values, the axial velocity coefficients from Figure 5 were used with kickdown angles from Figure 7. For the full-scale coefficients shown, engine axial thrust data were used in combination with engine biased kickdown angles (scale-model values plus  $1.8^\circ$ ) to reflect the results of the tuft surveys.

Table IV. Comparison of "D" Nozzle Geometric Characteristics with Predictions.

Side Door Angle, $\alpha$	"D" Nozzle Physical Exit Area				Nozzle Kickdown Angle $\theta_j$	
	Predicted		Measured		Predicted	Measured
	m <sup>2</sup>	(in. <sup>2</sup> )	m <sup>2</sup>	(in. <sup>2</sup> )		
0°	1.562	(2421)	1.577	(2444)*	8.05°	-
5°	1.623	(2516)			9.2°	-
10°	1.686	(2613)			10.3°	-
15°	1.750	(2713)			11.2°	-
20°	1.817	(2816)			11.9°	-
25°	1.886	(2924)			12.45°	** 14.25° (N <sub>F</sub> = 3000 rpm) 13.3° (Idle rpm)
30°	1.960	(3038)			12.75°	-
40°	2.119	(3285)			12.4°	-
<p>*Cold measured value was 1.570 m (2433 in.<sup>2</sup>), 1.577 m<sup>2</sup> (2444 in.<sup>2</sup>) includes thermal growth effects.</p> <p>**Average angles from exit plane tuft survey.</p>						

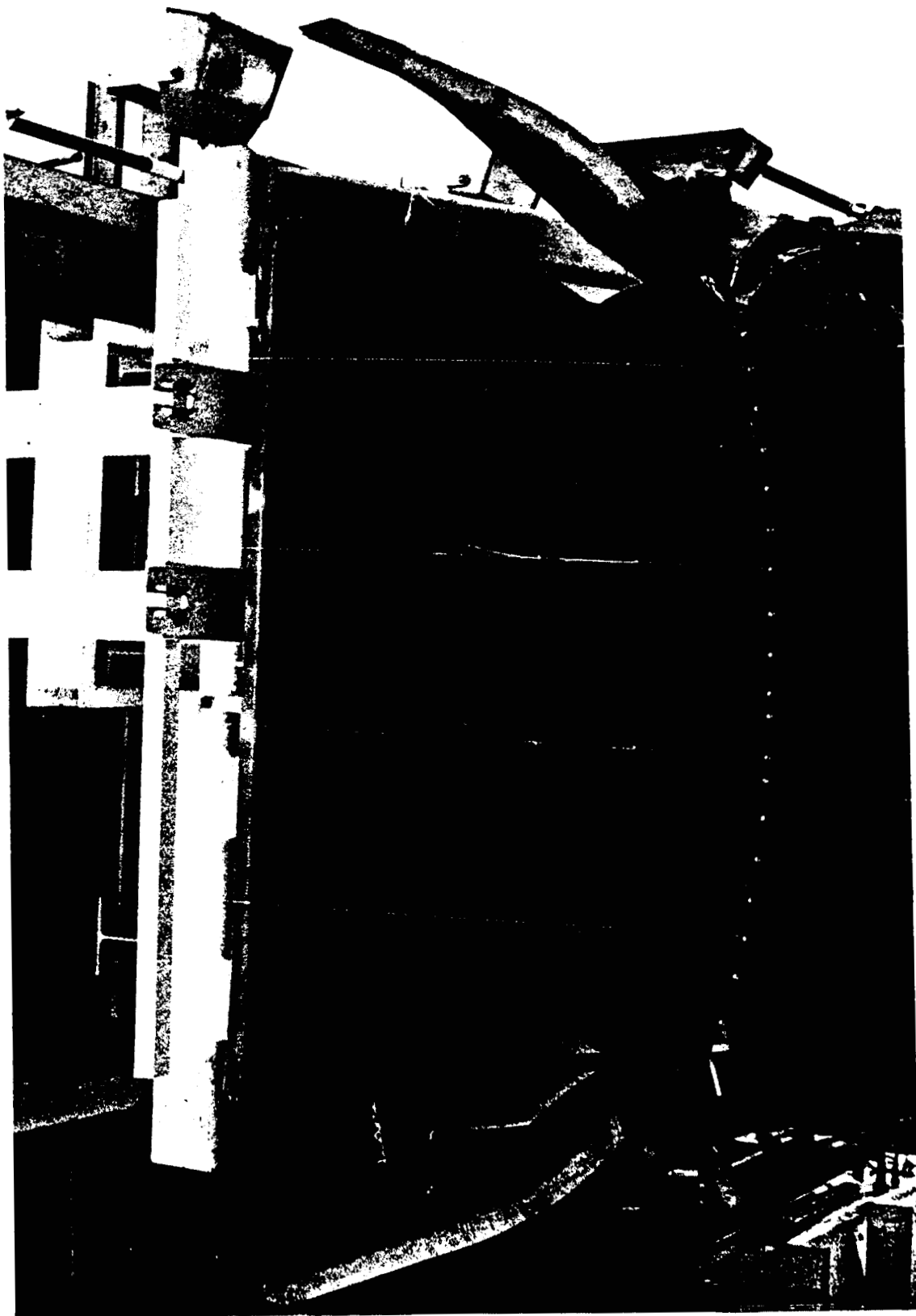


Figure 19. "D" Nozzle Exit Plane Tuft Pattern Orientation.

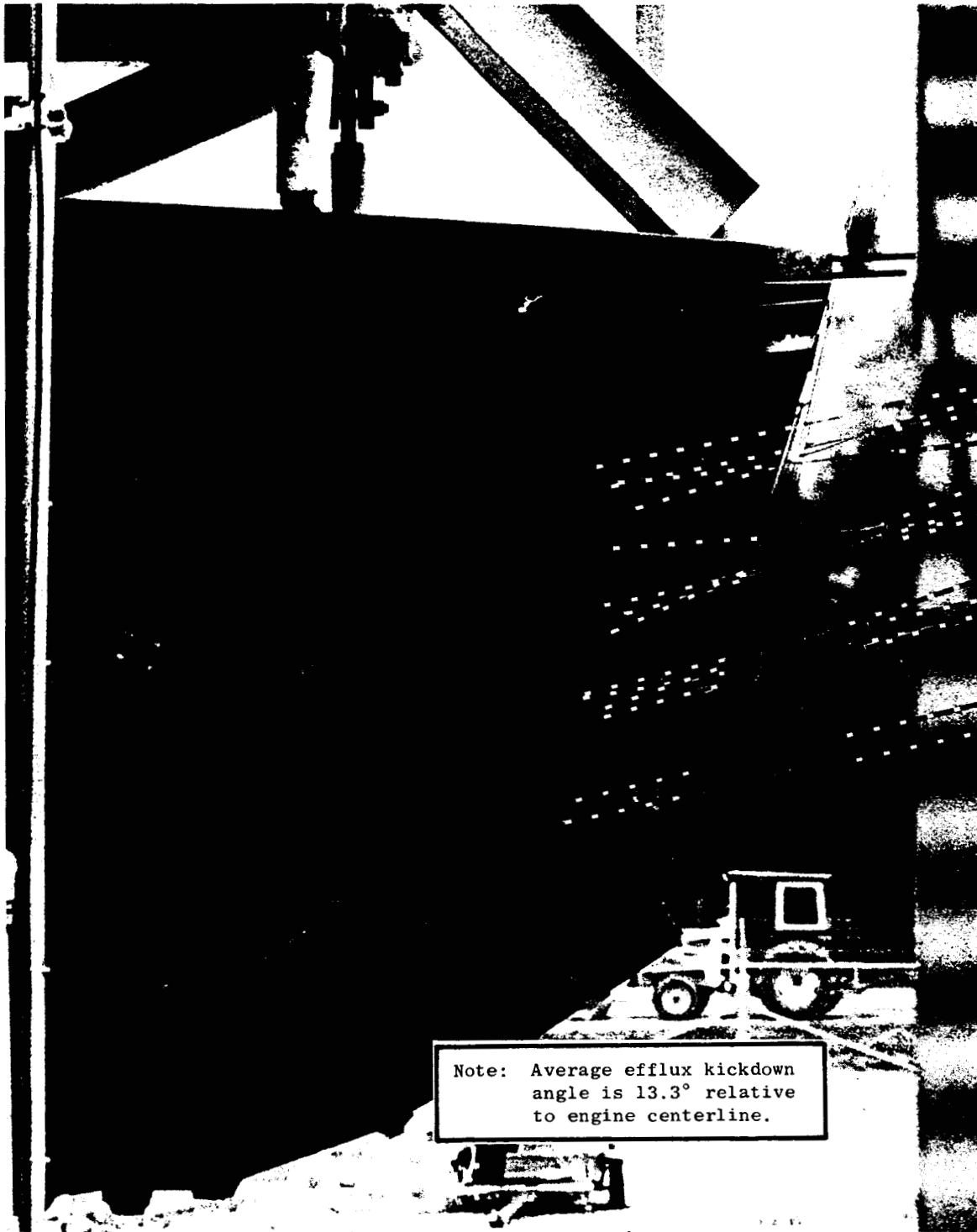


Figure 20. "D" Nozzle Tuft Survey at Idle Power.

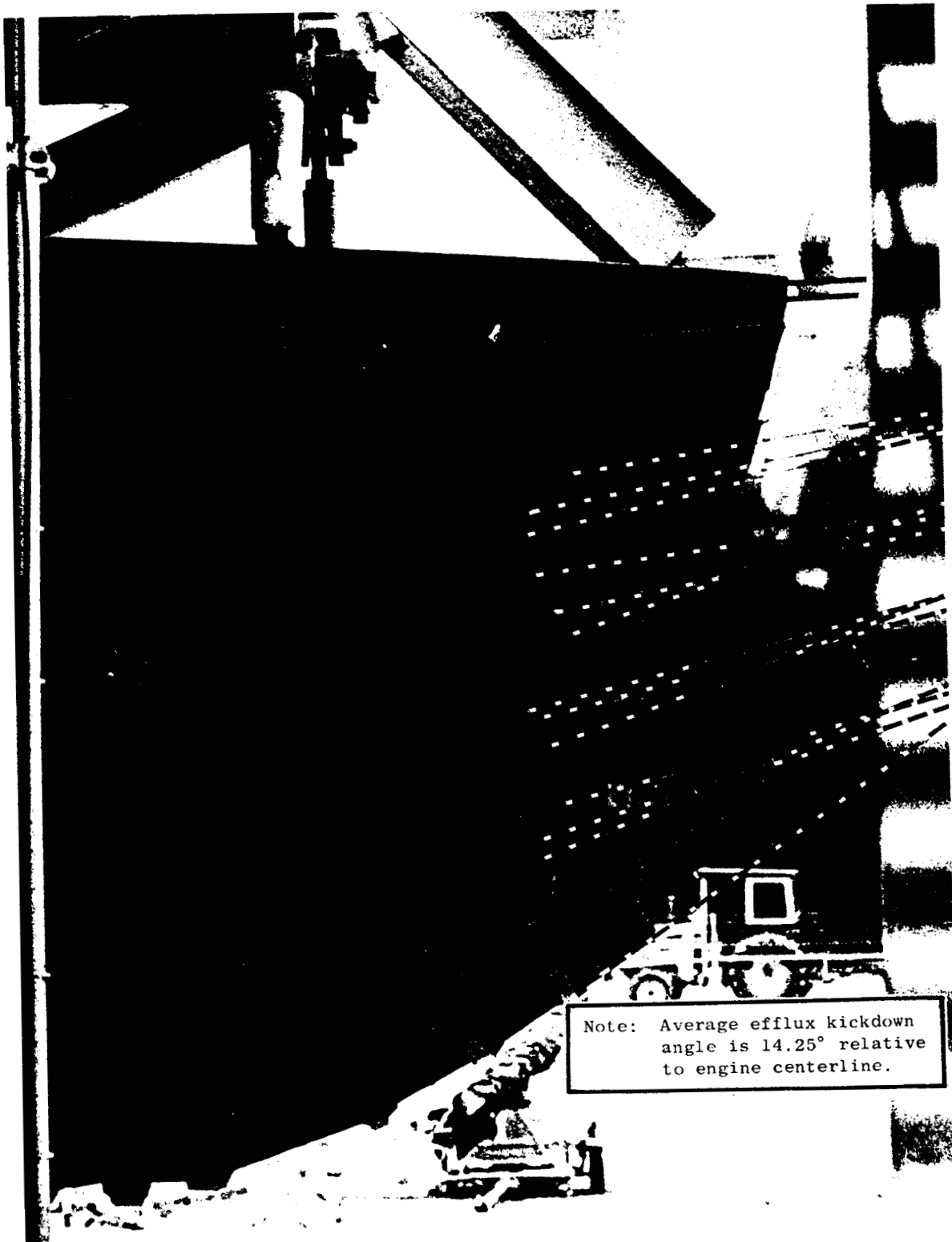


Figure 21. "D" Nozzle Tuft Survey at 3000 rpm Fan Speed.



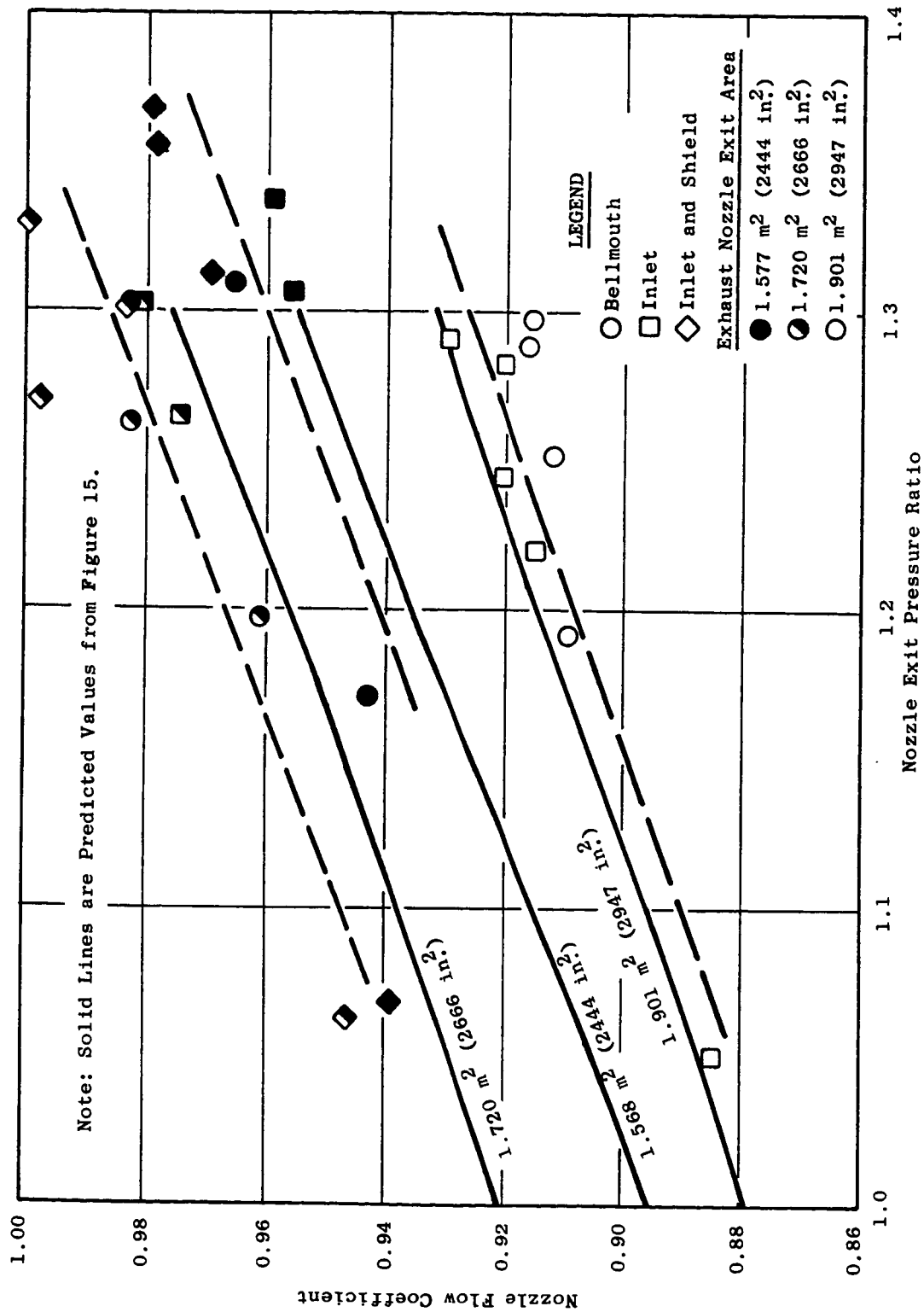


Figure 22. QCSEE OTW Engine "D" Nozzle Flow Coefficients.

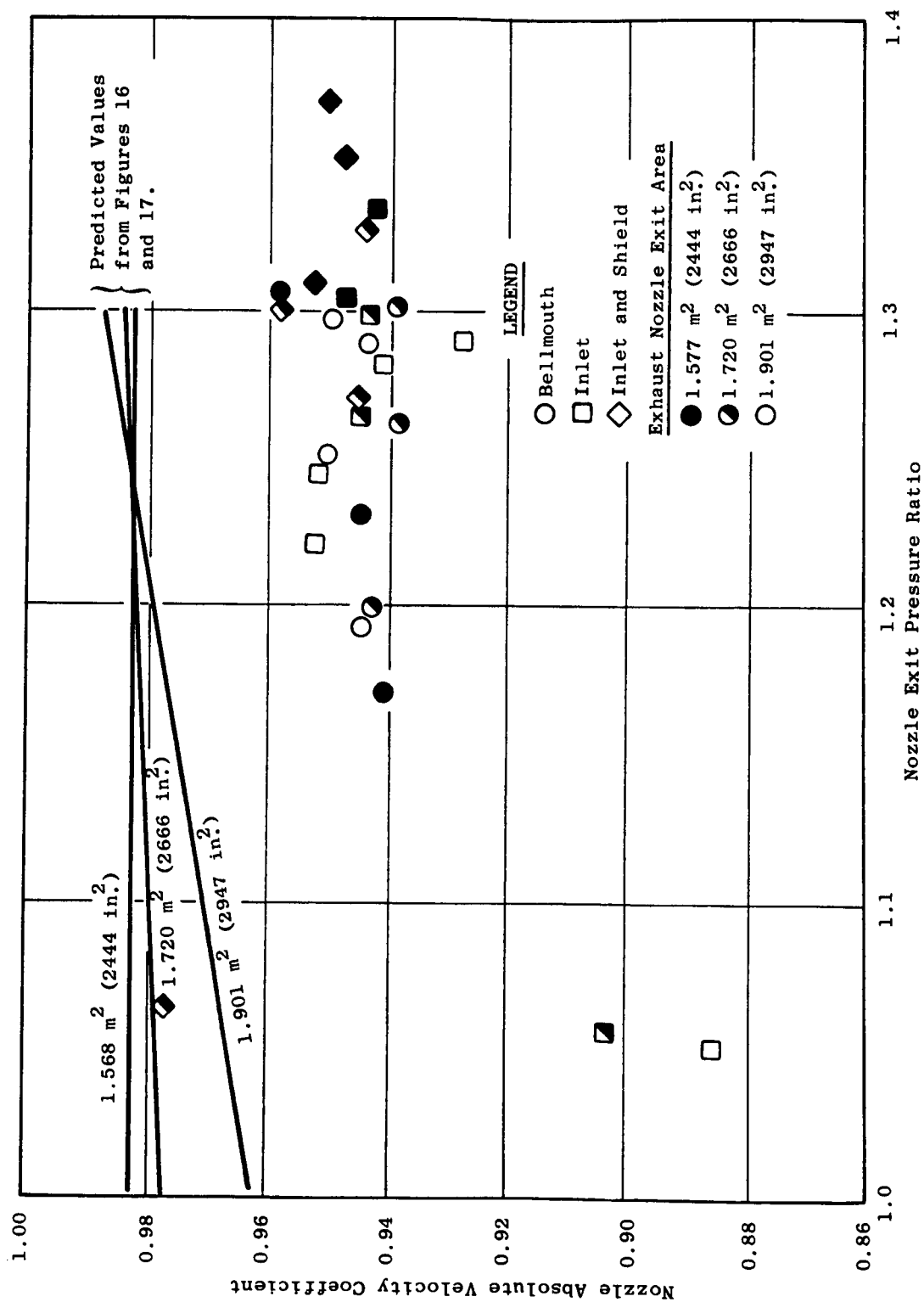


Figure 23. QCSEE OTW Engine "D" Nozzle Velocity Coefficients.

Comparison of full-scale measured and predicted values shows the full-scale velocity coefficients to be about four points lower ( $\Delta C_v \approx -0.04$ ) than predicted. The reason for this disparity is unknown, but it may be attributable to a compounding of small errors in determination of individual exhaust gas properties (flows, pressures, and temperatures), or in the full-scale thrust readings themselves, or in the accuracy of the scale-model results.

Despite the disparity in coefficient level, the relative insensitivity of measured velocity coefficient to either nozzle pressure ratio (particularly in the 1.2 to 1.3 region) or nozzle area, as indicated from the prediction, was substantiated.

#### 5.2.4 Exit Traverse Data

The "D" nozzle exit plane flow field at station 383 was traversed with total pressure and total temperature probes at locations 10.2 cm (4 inches) and 50.8 cm (20 inches) from the engine vertical centerline. The traverses were made in the region extending from the nozzle floor to just beyond the engine horizontal centerline plane. This region covered the maximum excursion capability of the traversing probes and mounting system available for OTW engine testing. Traverse data were used to determine jet velocity data for acoustical analysis. These data were generated at approximately 91% fan speed. Table V presents the total pressure and total temperature data obtained at 2.54-cm (1 in.) increments of the traversed regions. Figure 24 shows the orientation of the traverse runs and selected points used to evaluate local jet velocities (indicated by • on the nozzle end view shown in Figure 24). Also shown on this figure are the resultant jet velocities. On the basis of these calculated velocity trends, the remaining untraversed region of the exhaust was estimated as an approximate mirror image of the traversed region (dashed line on the velocity grid) for the 10.2 and 50.8 cm (4 and 20 inch) traverse planes. As indicated, fan and core velocity data both agree well with ideal calculated velocities, indicating that engine cycle duct loss estimates from fan and low pressure turbine rake planes are properly modeled in the QCSEE OTW engine cycle deck representation.

#### 5.2.5 Reverser Performance

As discussed in Section 3.0, the QCSEE reverser was found to meet the 35% objective reverse-thrust level (see Figure 9, Section 3.6) at a corrected fan speed of 81% for both blocker door settings (105° reference angle and 115° reference angle). As was pointed out in Section 3.6, fan airflows under these conditions were 299 kg/sec (660 lb/sec) and 281 kg/sec (620 lb/sec) respectively. On the basis of these data and the aerodynamic fan map shown on Figure 10 in Section 4, it becomes obvious that the reverser system, as predicted, forces the QCSEE engine to operate in a back-pressured state, in reverse mode, relative to the desired takeoff nozzle area operating conditions. Comparing fan map and measured airflow data at 81% fan speed

Table V. QCSEE OTW Engine Nozzle Exit Traverse Data; Corrected Fan Speed = 91%.

Kiel Probe Immersion From Nozzle Floor cm (in.)	10.2 cm (4.0 in.)				50.8 cm (20.0 in.)			
	P <sub>t</sub>		T <sub>t</sub>		P <sub>t</sub> *		T <sub>t</sub>	
	kN/m <sup>2</sup>	(lbf/in. <sup>2</sup> )	K	(° R)	kN/m <sup>2</sup>	(lbf/in. <sup>2</sup> )	K	(° R)
2.54 (1)	118.487	(17.185)	439.8	(791.7)	121.245	(17.585)	339.8	(611.7)
5.08 (2)	120.556	(17.485)	487.0	(876.6)	122.279	(17.735)	356.5	(641.7)
7.62 (3)	121.245	(17.585)	573.2	(1031.7)	121.934	(17.685)	378.7	(681.7)
10.16 (4)	122.624	(17.785)	650.9	(1171.7)	121.934	(17.685)	437.0	(786.7)
12.70 (5)	123.934	(17.975)	700.9	(1261.7)	122.279	(17.735)	423.1	(761.7)
15.24 (6)	123.658	(17.935)	823.1	(1481.7)	124.692	(18.085)	467.6	(841.7)
17.78 (7)	122.624	(17.785)	900.9	(1621.7)	124.692	(18.085)	473.1	(851.7)
20.32 (8)	121.245	(17.585)	950.9	(1711.7)	124.692	(18.085)	467.6	(841.7)
22.86 (9)	121.245	(17.585)	962.0	(1731.7)	123.313	(17.885)	416.5	(749.7)
25.40 (10)	121.934	(17.685)	973.1	(1751.7)	125.037	(18.135)	372.0	(669.7)
27.94 (11)	121.934	(17.685)	973.1	(1751.7)	125.382	(18.185)	352.6	(634.7)
30.48 (12)	121.934	(17.685)	973.1	(1751.7)	128.140	(18.585)	322.0	(579.7)
33.02 (13)	122.624	(17.785)	973.1	(1751.7)	128.829	(18.685)	305.4	(549.7)
35.56 (14)	122.624	(17.785)	867.6	(1561.7)	128.829	(18.685)	305.4	(549.7)
38.10 (15)	124.692	(18.085)	739.8	(1331.7)	128.829	(18.685)	302.6	(544.7)

\* Barometer = 97.773 kN/m<sup>2</sup> (14.185 lbf/in.<sup>2</sup>)

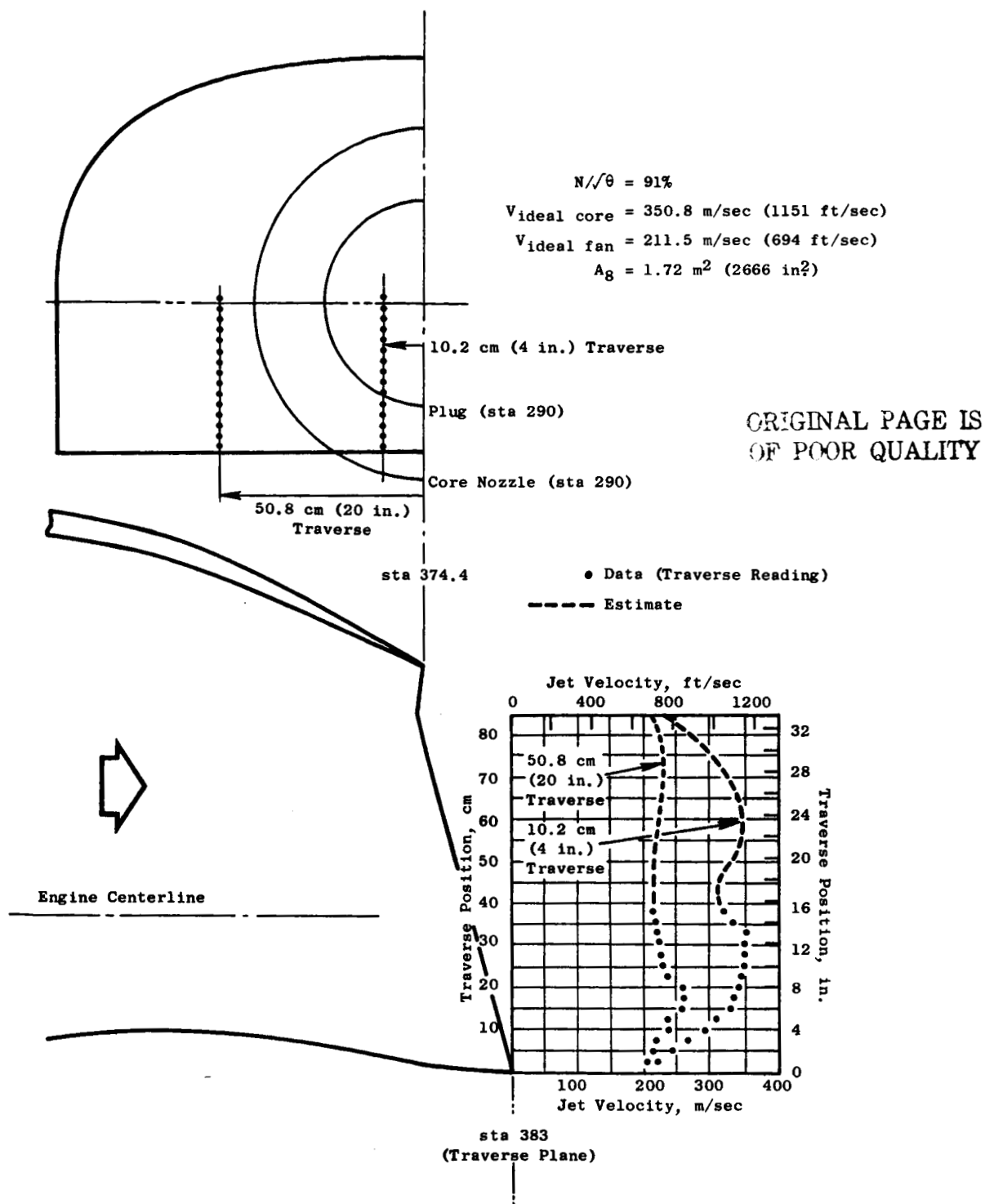


Figure 24. QCSEE OTW Engine Exit Velocity Profiles.

shows the desired flow for no back-pressuring would be 340 kg/sec (750 lbs/sec) at a takeoff area of  $1.9 \text{ m}^2$  (2947 in.<sup>2</sup>), while measured reverse-mode values were 299 kg/sec (660 lb/sec) and 281 kg/sec (620 lb/sec). Under these conditions fan map operating lines fall below the cruise nozzle area setting of  $1.577 \text{ m}^2$  (2444 in.<sup>2</sup>). In fact, the 115° blocker door setting data appears to lie along the estimated fan stall line on the Figure 10 fan map of Section 4. This is consistent with stall/stress trends observed during Peebles testing.

The observed back-pressuring could be considerably reduced if the Mach number entering the reverser were lowered. This would require a larger nacelle cross section at this station and would preclude using the same fan cowl door hardware as used for the UTW engine.

## REFERENCES

1. Advanced Engineering and Technology Programs Department, "Quiet Clean Short-Haul Experimental Engine (QCSEE). The Aerodynamic and Mechanical Design of the QCSEE Over-the-Wing Fan," General Electric Company, NASA CR-134915, April 1976.
2. Advanced Engineering and Technology Programs Department, "Quiet Clean Short-Haul Experimental Engine (QCSEE) Under-the-Wing Propulsion System Test Report," General Electric Company, Publication Pending.
3. Advanced Engineering and Technology Programs Department, "Quiet Clean Short-Haul Experimental Engine (QCSEE) Over-the-Wing (OTW) Final Design Report," General Electric Company, NASA-CR-134848, June 1977.
4. Advanced Engineering and Technology Programs Department, "Analysis and Documentation of QCSEE (Quiet Clean Short-Haul Experimental Engine) Over-the-Wing Exhaust System Development," General Electric Company, NASA-CR-2792, December 1976.

# DISTRIBUTION LIST

AIResearch Division  
Garret Corporation  
F.B. Wallace  
P.O. Box 5217  
Phoenix, Arizona 85010

American Airlines  
Maintenance and Engineering Center  
K. Grayson  
Tulsa, Oklahoma 74151

Andrews Air Force Base  
Lt. Col. G. Strand  
AFSC Headquarters  
Washington, D.C. 20334

AVCO/Lycoming  
S. Deckert  
550 S. Main Street  
Stratford, Connecticut 06497

The Boeing Company  
H. Higgins  
P.O. Box 3999  
Seattle, Washington 98124

The Boeing Company  
Wichita Division  
D. Torkelson  
Wichita, Kansas 67210

Bolt, Beranek and Newman, Inc.  
R. Hayden  
50 Moulton Street  
Cambridge, Massachusetts 02138

Curtiss-Wright Corporation  
Power Systems Division  
W. Johnson  
One Passaic Street  
Wood Ridge, New Jersey 07075

Department of Transportation  
NASA/DOT Joint Office of Noise  
Abatement  
C. Foster  
Office of Secretary  
Washington, D. C. 20590

Detroit Diesel Allison Division  
of General Motors  
F. Walters  
Suite 312  
333 West First Street  
Dayton, Ohio 45402

Douglas Aircraft Company  
L. Malthan  
3855 Lakewood Boulevard  
Long Beach, California 90801

Environment Protection Agency  
J. Schettino  
1835 "K" Street, NW  
Washington, D.C. 20460

Federal Aviation Administration  
Noise Abatement Division  
J. Woodall  
Washington, D.C. 20590

General Dynamics Convair Division  
G. Nicoloff  
San Diego, California 92112

Grumman Aerospace Corporation  
C. Hoeltzer  
South Oyster Bay Road  
Bethpage, New York 11714

Hamilton Standard  
Division of United Aircraft  
A. Jackson  
Windsor Locks, Connecticut 06096

Lockheed Aircraft Corporation  
T. Higgins  
Burbank, California 91503

Lockheed Georgia Company  
H.S. Sweet  
Marietta, Georgia 30060

## NASA Installations

NASA Headquarters  
N.F. Rekos  
Washington, D.C. 20546

NASA-Ames Research Center  
L. Roberts  
Moffett Field, California 94035

NASA-Flight Research Center  
D.R. Scott  
Edwards, California 93523

NASA-Langley Research Center  
R. Kuhn  
Hampton, Virginia 23665

NASA-Lewis Research Center  
21000 Brookpark Road  
Cleveland, Ohio 44135

M.A. Beheim  
D.N. Bowditch  
L.J. Chelko  
C.C. Ciepluch  
E.W. Conrad  
R.J. Denington  
A. Ginsburg  
M.J. Hartmann  
R.H. Kemp  
Lewis Library  
R.W. Luidens  
D.L. Nored  
Report Control Office  
L.W. Schopen  
R.W. Schroeder  
M.F. Valerino

NASA/Air Force Liaison  
Wright Patterson Air Force Base  
Dayton, Ohio 45433

L. Obery  
C. Simpson  
Col. C.E. Painter  
G.K. Richey  
G.P. Peterson

Pratt & Whitney Aircraft  
Division of United Aircraft Corp.  
J. Chew  
20800 Center Ridge Road  
Rocky River, Ohio 44116

Rohr Corporation  
F. Hom  
Box 878  
Foot and H Street  
Chula Vista, California 92012

Wyle Laboratories  
L. Sutherland  
128 Maryland Street  
El Segundo, California 90245

Rockwell International  
Los Angeles Division  
Attn: D. Schlundt  
International Airport  
Los Angeles, California 90009